Advances in Bone Marrow Imaging: Strengths and Limitations from a Clinical Perspective

Charbel Mourad, MD, PhD[1,2] Aurelio Cosentino, MD[3] Marie Nicod Lalonde, MD[4] Patrick Omoumi, MD, PhD[1]

[1] Department of Radiology, Lausanne University Hospital and University of Lausanne, Lausanne, Switzerland
[2] Department of Diagnostic and Interventional Radiology, Hôpital Libanais Geitaoui- CHU, Beyrouth, Lebanon
[3] Department of Radiology, Hôpital Riviera-Chablais, Vaud-Valais, Rennaz, Switzerland
[4] Department of Nuclear Medicine and Molecular Imaging, Lausanne University Hospital and University of Lausanne, Lausanne, Switzerland

Address for correspondence Patrick Omoumi, MD, PhD, Department of Diagnostic and Interventional Radiology, CHUV, Lausanne, Switzerland (e-mail: Patrick.omoumi@chuv.ch).

Semin Musculoskelet Radiol 2023;27:3–21.

Abstract

Conventional magnetic resonance imaging (MRI) remains the modality of choice to image bone marrow. However, the last few decades have witnessed the emergence and development of novel MRI techniques, such as chemical shift imaging, diffusion-weighted imaging, dynamic contrast-enhanced MRI, and whole-body MRI, as well as spectral computed tomography and nuclear medicine techniques. We summarize the technical bases behind these methods, in relation to the common physiologic and pathologic processes involving the bone marrow. We present the strengths and limitations of these imaging methods and consider their added value compared with conventional imaging in assessing non-neoplastic disorders like septic, rheumatologic, traumatic, and metabolic conditions. The potential usefulness of these methods to differentiate between benign and malignant bone marrow lesions is discussed. Finally, we consider the limitations hampering a more widespread use of these techniques in clinical practice.

Keywords
- Dixon
- diffusion-weighted imaging
- dynamic contrast-enhanced magnetic resonance imaging
- whole-body magnetic resonance imaging
- dual-energy computed tomography

Bone marrow disorders cover a wide range of conditions, such as neoplastic, septic, rheumatologic, traumatic, and metabolic disorders. Although conventional magnetic resonance imaging (MRI) remains the modality of choice for their assessment, the last few decades have seen the emergence of novel MRI techniques: chemical shift imaging (CSI), diffusion-weighted imaging (DWI), dynamic contrast-enhanced (DCE) MRI, and whole-body MRI, along with spectral computed tomography (CT) and nuclear medicine techniques.

These developments have been the focus of an increasing body of literature, with promising results covering both qualitative and quantitative analyses in a variety of conditions.

To understand how these techniques can be applied to various clinical scenarios, we provide an overview of their technical basics in relation to common physiologic and pathologic processes involving the bone marrow. Based on a review of the relevant literature, we discuss the strengths

Issue Theme Nontumor Marrow Changes; Guest Editors, Patrick Omoumi, MD, PhD and Bruno Vande Berg, MD, PhD

DOI https://doi.org/10.1055/s-0043-1761612.
ISSN 1089-7860.

Thieme Medical Publishers, Inc., 333 Seventh Avenue, 18th Floor, New York, NY 10001, USA

and limitations of these imaging methods to assess the most common non-neoplastic conditions and to differentiate them from neoplastic conditions, keeping the focus on clinical utility (►**Table 1**).

Fat, Cellularity, and Vascularity: Bone Marrow Physiologic and Pathologic Changes Relevant to Marrow Imaging

To understand the contribution of different imaging techniques in investigating normal and pathologic conditions of bone marrow, following is a review of the basics of marrow pathophysiology.

First, normal bone marrow, whether yellow or red, contains a variable amount of fat. The proportion of water and fat content varies depending on the composition of bone marrow, related to several physiologic processes (including the transformation of red-to-yellow marrow with age, premenopausal status, etc.). In pathologic conditions the proportion of water and fat also changes with water content increasing relative to fat content. CSI and magnetic resonance spectroscopy (H1-MRS) can probe the fat content and quantify it to differentiate marrow-replacing lesions (where marrow fat is replaced, due to the presence of either malignant or benign lesions) from non–marrow-replacing lesions (where marrow fat is preserved, usually in relation to a benign lesion). Dual-energy computed tomography (DECT) and virtual non-calcium (VNCa) reconstructions can analyze bone marrow water and fat content by suppressing the attenuation component of mineralized bone, thanks to tissue characterization based on the atomic number Z and the photoelectric effect.

Second, many pathologic marrow conditions are characterized by increased water content, decreased fat content, increased vascularity, and destruction of the trabecular bone structure, all of which lead to increased diffusivity. DWI exploits the Brownian motion of water molecules and is sensitive to conditions where this motion is altered. The apparent diffusion coefficient (ADC) enables a quantitative evaluation of diffusion restriction.

Third, marrow pathologies show increased vascularity that may be assessed by DCE-MRI.

Finally, nuclear medicine and metabolic imaging examine the distribution of specific components of the hematopoietic and reticuloendothelial systems or the metabolic activity in bone marrow.

Chemical Shift Imaging

Technique

CSI takes advantage of the slight difference in resonance frequency that exists between water and fat protons to provide a series of four sets of images: in-phase (IP), out-of-phase (OP), water only (WO), and fat only (FO). Although Dixon described it in the 1980s, it has only recently become possible to associate this method with spin-echo–based sequences, the backbone of musculoskeletal MRI protocols, opening the door for multiple applications in this field.

CSI MRI can also be used to probe bone marrow fat content quantitatively, by measuring the signal drop between IP and OP images or by calculating the fat fraction (FF). This can be done both on gradient-echo and spin-echo sequences.

Normal Bone Marrow

The variation of signal intensity in normal bone marrow parallels the relative amount of water and fat protons, itself correlated to the relative amount of red and yellow bone marrow. Just as for T1-weighted sequences, red marrow presents lower signal intensity than yellow marrow on FO images due to its lower fat content. Furthermore, red marrow is lower in signal intensity on T2 IP images than red marrow.

At quantitative analysis, normal bone marrow shows a significant drop in signal intensity due to the presence of fat protons that at least partially cancel the signal of water, with a wide range of normal values due to variable marrow composition. It is reported that normal bone marrow should present a drop of at least 20% on OP compared with IP images.[1,2] The mean FF for normal vertebral marrow varies greatly, ranging between 13.7% and 83% (mean: $50.51 \pm 14.69\%$).[3] FF of normal bone marrow varies with age, sex, and menstrual status; premenopausal women have higher marrow cellularity than men, whereas bone marrow fat increases with age in both sexes.[4]

Clinical Applications

Robust Fat Suppression Technique

The Dixon method has mostly been used as a fat suppression technique that has proved to be more robust to magnetic field inhomogeneities than chemical shift selective suppression (CHESS) while providing a better signal-to-noise ratio than short tau inversion recovery (STIR) sequences.[5,6] Therefore, it is an appealing technique for large field-of-view (FOV) imaging of the bone marrow.

Optimization of Magnetic Resonance Imaging Protocols

The four sets of images generated by a Dixon sequence can be used to optimize MRI protocols, particularly when using a fast spin-echo (FSE) T2-weighted Dixon sequence. Through a single acquisition, both fat-suppressed and non–fat-suppressed fluid-sensitive images can be obtained. IP T2 images are equivalent to T2 FSE images, whereas WO images correspond to fat-suppressed T2 images. Furthermore, FO T2 images are not only sensitive but also specific to the signal of fat and can substitute T1-weighted images for the assessment of tissue fat content.[7–11] The potential of T2 FO images to replace T1-weighted images has been validated in a few studies addressing lesion detection in multiple myeloma,[8] metastases,[9,12] and characterization of vertebral compression fractures (VCFs).[13] For the common scenario of MRI in the context of nonspecific low back pain, a single sagittal T2-weighted Dixon sequence may replace the combination of T1-weighted, T2-weighted, and fat-suppressed T2-weighted sequences.[7,10,14] Of note, quantitative information on bone marrow fat content is also readily available when using Dixon sequences.

Table 1 Strengths and limitations of advanced imaging techniques in common clinical applications

	Rationale for use	Normal marrow	Lesion detection and characterization	VCF	Infection	Inflammation	Metabolic	Other application	Pitfalls and limitations
CSI	Benign conditions contain residual fat	-SI drop on OP images -High but variable fat content	-Fat-only images have high CNR for detection of focal lesions -Marrow-replacing lesions: < 20% decreased SI on OP	> 20% decreased SI on OP images suggests a benign VCF		Detection of inflammatory and structural lesions in a single acquisition (T2-Dixon)	-Higher marrow adiposity in osteoporosis	-Protocol optimization by providing fat-sensitive and fluid-sensitive images on single T2-Dixon sequences (spine metastases, degenerative spine, spondyloarthritis)	-False positive in tuberculous spondylitis and sclerotic lesions
DWI	Increase in marrow cellularity and abscesses cause restricted Brownian motion	-Signal on DWI is variable (age, sex, Hb) -ADC of normal bone marrow: 0.2–0.6 $\times 10^{-3}$ mm^2/s	-Malignant and benign lesions have higher ADC than normal marrow	-Overlap of ADC values between benign and malignant VCF	-DWI may distinguish BME from osteomyelitis -DWI may detect abscesses if contrast injection contraindicated -DWI could differentiate between diabetic neuroarthropathy and osteomyelitis. Overlap exists	-Claw sign on lumbar MRI: Modic type 1 -DWI inferior to regular protocol of sacroiliitis	Limited value in osteonecrosis		-Variable protocols among different vendors and institutions -DWI is not a robust tool to differentiate infection from malignancy -DWI should be interpreted in conjunction with standard MRI sequences
DCE-MRI	-Tumors present neoangiogenesis -Inflammatory conditions present increased vascularity	-Physiologic differences in marrow perfusion	-Fractional plasma volume lower in neoplastic lesions	-Pathologic VCF has higher perfusion parameters	K^{trans}, K_{ep}, and V_e higher in osteomyelitis than in diabetic neuroarthropathy - K_{ep} higher in malignant compared with tuberculous lesions -Tuberculous lesions do not show washout		-Marrow perfusion decreases in osteoporosis and around osteonecrotic lesions (ischemic penumbra)		-Frequent false positives and false negatives in VCF -Limited reproducibility of cut-off values between vendors and techniques
Spectral CT imaging	-Attenuation of tissues depends on atomic number Z; mineralized bone can be suppressed from images (VNCa images)	No standard HU values	-VNCa may improve detection of multiple myeloma and metastases	-VNCa images detect BME in acute VCF		-Detection of BME in sacroiliitis		-Detection of BME in trauma	-Validation of an established diagnostic threshold is difficult because of variety of acquisition and postprocessing techniques -Sensitivity of DECT in the diagnosis of acute but morphologically occult fractures remains to be addressed -False positives and false negatives are frequent
Nuclear medicine	-Bone marrow metabolism (FDG-PET) -Distribution in the hematologic system (WBC scintigraphy)				-High diagnostic accuracy in periprosthetic infection and in fracture-related infections (WBC scintigraphy) -Search for a focus of infection in FUO (FDG-PET)				-Intense uptake of red bone marrow hampers detection of bone marrow infection in the axial skeleton (WBC scintigraphy) -Focal increased uptake in benign marrow hyperplasia (FDG-PET)

Abbreviations: ADC, apparent diffusion coefficient; BME, bone marrow edema-like; CNR, contrast-to-noise ratio; CSI, chemical shift imaging; CT, computed tomography; DCE-MRI, dynamic contrast-enhanced MRI; DECT, dual-energy computed tomography; DWI, diffusion-weighted imaging; FDG, fluorodeoxyglucose; FUO, fever of unknown origin; Hb, hemoglobin; HU, Hounsfield Units; K_{ep}, rate constant; K^{trans}, volume transfer constant; MRI, magnetic resonance imaging; OP, out-of-phase; PDFF, proton-density fat fraction; PET, positron emission tomography; SI, signal intensity; VCF, vertebral compression fracture; V_e, extra vascular space; VNCa, virtual non-calcium images; WBC, white blood cells.

Lesion Characterization and Evaluation of Vertebral Compression Fractures

On standard MRI, the interpretation of decreased signal intensity on T1-weighted sequences is based on a comparison with an intrinsic reference (the signal intensity of muscles), and it helps discriminate between non–marrow-replacing lesions (T1 signal $\geq$ muscle/disk), which are usually benign, and marrow-replacing lesions (T1 signal $<$ muscle/disk)[15–17] (►**Fig. 1**). This comes with a few caveats: the signal intensity of muscle and disks that serve as a reference can be altered, whereas some marrow-replacing lesions may be spontaneously high in signal intensity (e.g., due to the presence of melanin or high protein content), leading to false negatives. The interpretation of FO images, which are fat specific, is more straightforward. The absence of high-intensity pixels within a lesion is suggestive of a marrow-replacing lesion, whereas non–marrow-replacing lesions contain high-intensity pixels.

As discussed earlier, gradient-echo and FSE Dixon images have been used to assess the fat content of bone marrow quantitatively. Most reports found a threshold of 20% to be effective in differentiating bone-marrow-replacing lesions (signal drop $\leq$ 20%) from non–bone-marrow-replacing, (signal drop $>$ 20%), which are usually benign.[1,2] The need for biopsy could be eliminated in $>$ 60% of patients with benign disease as demonstrated in a monocentric study.[18] In addition, CSI is useful to confirm the diagnosis of focal hematopoietic bone marrow islands and avoid unnecessary follow-up.[19] However, the measurement may depend on the types of sequences used, and other thresholds have occasionally been reported.[20]

A quantitative evaluation of intralesional fat through the calculation of FF maps, either with gradient-echo or spin-echo–based sequences, has also shown potential to differentiate benign from malignant lesions accurately.[3,21,22]

Axial Spondyloarthropathy

A single T2-weighted Dixon sequence was shown to provide all the information to assess inflammatory and structural lesions of spondylarthritis in the spine and sacroiliac joints, and it may replace standard T1 and fat-suppressed fluid-sensitive sequences[23,24] (►**Fig. 2**). The robust fat suppression and reduced examination time are additional assets for large FOV acquisitions.

Miscellaneous Marrow Conditions

Quantitative studies of marrow adiposity in osteoporosis showed increased marrow fat fraction with age and with decreased bone mineral density.[25–27] In clinical research, FF could be used as a biomarker for osteoporosis, knowing there is an overlap with healthy subjects.[27] In addition, some authors used OP images to detect ankle and foot fractures,[28] measure tumor size,[29] and assess femoral head osteonecrosis.[30] However, it is important to mention that the hypointense lines referred to as "India ink artifacts" seen on the OP images correspond to areas with an equal amount of water and fat protons and should not be mistakenly interpreted as fracture lines.

Pitfalls

Dixon images, especially two-point techniques, are prone to fat-water swapping artifact that could be easily characterized as such by a side-to-side comparison of FO and WO images.

Areas that contain a disproportionate amount of water protons relative to fat protons (such as in cysts, abscesses, and Schmorl's nodes) intrinsically have low or no signal drop on OP images, potentially leading to false-positive results[31] (►**Fig. 3**). Sclerotic metastases have also been shown to be a potential source of false-positive results, whose cause might be multifactorial[31] (►**Fig. 3**).

Another pitfall is hypocellular neoplasia, such as in multiple myeloma, where the presence of substantial remaining fat may lead to false-negative FF findings.[3,32]

Finally, FF measurements depend on the acquisition method used and their relative sensitivity to T1, T2, and $T2^*$ decay,[4,33] in addition to the lack of standardization and variable thresholds that have been used across studies.[3,21,22] These limitations apply to most currently available quantitative applications. As a rule, overreliance on quantitative assessments should be avoided and quantitative information should rather be used as an adjunct to, rather than a substitute for qualitative assessment, when necessary.

Diffusion-weighted Imaging

Technique

DWI assesses the self-diffusion, that is, the Brownian motion of water molecules, influenced by the microscopic structure and organization of biological tissues. The DWI signal is influenced by the choice of the sequence and the strength of the diffusion weighting given by the b-value. If two or more images with different b-values are acquired, a quantitative measurement of diffusion may be obtained: the ADC.[34]

Most clinical DWI examinations are performed with diffusion-weighted single-shot spin-echo echo planar imaging (EPI) sequences, which have the advantage of being fast, and therefore relatively robust against motion artifacts.[35] However, EPI sequences have limited spatial resolution (i.e., 128×128 pixels), increased susceptibility to magnetic field inhomogeneities, and eddy currents.[35] They are prone to significant image distortion and susceptibility artifacts due to the presence of the cortical bone–fat interface, and the vicinity to the lungs and great vessels.[36] Single-shot reduced FOV EPI can reduce geometric distortion effects but reduces signal-to-noise ratio and therefore requires longer scan times.[36] Multishot readout-segmented EPI sequences were more recently proposed to decrease susceptibility and motion artifacts compared with single-shot EPI, with reasonable scanning times.[37]

Of importance, the presence of fat reduces ADC values, and the use of fat suppression techniques is usually required.[34,35]

Normal Bone Marrow

The ADC values of normal vertebral bone marrow range between 0.2 and 0.6×10^{-3} mm^2/s.[35,38] These variations are partly explained by technical parameters, such as

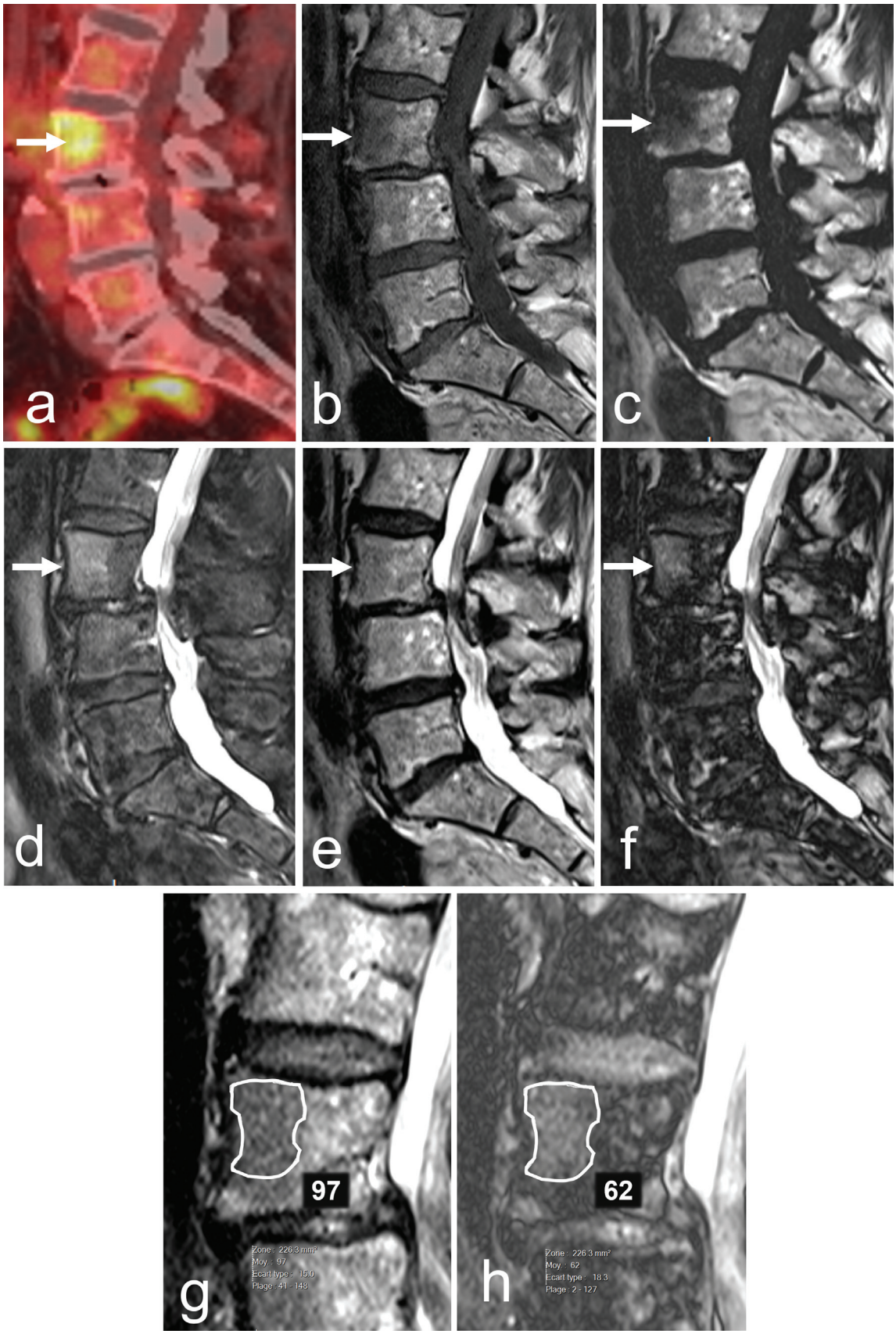

Fig. 1 A 74-year-old woman with ovarian adenocarcinoma. (**a**) Sagittal reformat of fused fluorodeoxyglucose positron emission tomography/computed tomography images showing focal uptake in L3 vertebral body (arrow; maximum standardized update value = 6). Sagittal (**b**) T1-weighted, (**c**) fat-only, (**d**) water-only, (**e, g**) in-phase, and (**f, h**) out-of-phase T2-weighted Dixon images. The lesion (arrows) contains fat with a drop in signal intensity of 36%, suggestive of a non–marrow-replacing lesion. (**g**) Note the low signal intensity on the non–fat-suppressed image that concurs with benign nodular marrow hyperplasia. The lesion was unchanged on subsequent follow-up studies.

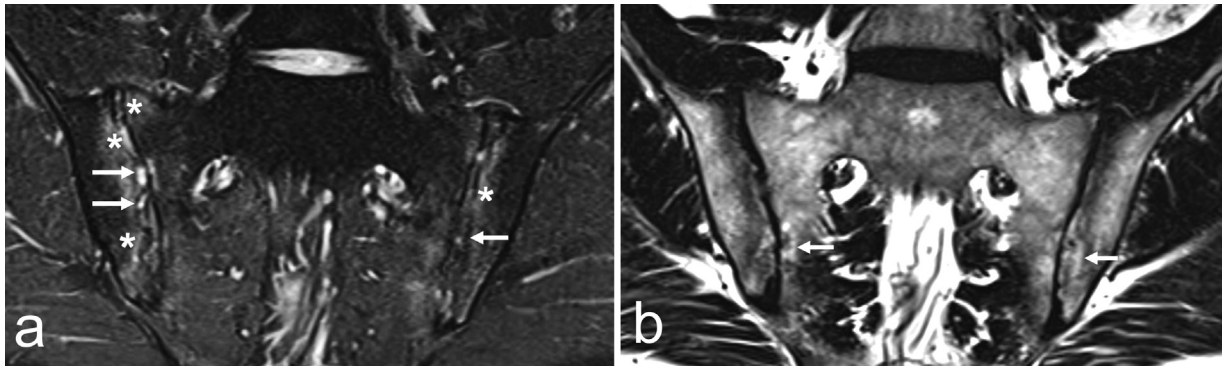

Fig. 2 A 34-year-old man with axial spondyloarthropathy. Coronal oblique (**a**) water-only and (**b**) fat-only images of a single T2-weighted Dixon show bone marrow edema-like signal intensity (a, white asterisks), subchondral erosions (a, arrows), and fat metaplasia (b, arrows). The T2-weighted Dixon technique enables accurate depiction of signs of disease activity and structural bone changes in a single acquisition.

differences in hardware, pulse sequences, diffusion weightings, and postprocessing.

In addition, the diffusion properties of normal bone marrow depend on physiologic parameters. The relative amount of fat and water influence the ADC values, with the ADC of fat close to zero.[34,35] Therefore, DWI of the normal bone marrow may vary depending on factors influencing the FF, including sex, age, premenopausal status, as well as anatomical location (axial versus peripheral skeleton, different vertebral levels, pelvic bones, etc.).[4,39,40] Any condition influencing the red versus yellow marrow distribution and the proportion of mineralized bone (osteoporosis, anemia) may influence DWI[35,40] (►**Fig. 4**).

Clinical Applications

Lesion Characterization and Evaluation of Vertebral Compression Fractures

Bone marrow lesions, whether benign or malignant, have higher ADCs than normal bone marrow. On one hand, this finding can be explained because normal bone marrow has a low signal on DWI and a low ADC value, mostly attributed to the high fat content and the presence of bone trabeculae. On the other hand, bone marrow lesions exhibit high tumoral cellularity, decreased FF, increased water content and vascularity, and disrupted trabeculae that likely contribute to the higher signal on DWI and higher ADC values. Thanks to the difference between normal marrow and malignant lesions, DWI has been established as a method of reference to assess bone marrow involvement in the oncologic setting.[41–43] DWI has also been used to differentiate between benign and malignant bone marrow lesions.

In a meta-analysis, differentiation between benign and malignant vertebral lesions based on quantitative analysis of ADC values had pooled sensitivity and specificity of 89% and 87%, respectively.[44] Note, however, that the group of benign lesions included a wide range of pathologies including infectious lesions, nodular hyperplastic bone marrow, and other primary bone lesions. Due to their different tissue characteristics, these lesions should present different ADC values (e.g., hyperplastic bone marrow has low ADC value due to the preserved bone and bone marrow structures), making the analysis difficult. For the differentiation of benign and malignant VCFs, ADC values yielded pooled sensitivity and specificity of 92% and 91%, respectively.[44] In practice, morphological analysis of VCFs most of the time is sufficient for the diagnosis,[13] and the added value of DWI in cases where morphological analysis is inconclusive remains to be determined.

Diabetic Foot

In diabetic patients, the distinction between pedal osteomyelitis and diabetic neuroarthropathy (Charcot's arthropathy) is challenging, and both conditions may coexist. Few studies have investigated the use of DWI in diabetic feet with discordant results. In two studies, ADC values were higher in diabetic neuroarthropathy than in osteomyelitis, suggesting a cut-off value of 0.98×10^{-3} mm^2/s to differentiate the two conditions,[45,46] whereas there was a significant overlap between the ADC values in a larger study that used a normalized signal intensity for ADC.[47] In a recently published study, a readout-segmented multishot echo planar DWI showed promising results to distinguish osteomyelitis from bone marrow edema (BME) related to other conditions, although there was again some overlap between the two groups, with a 95% accuracy achieved in only 73% of cases.[37]

Spinal Infections

In vertebral end endplates with BME, on visual inspection of DWI, the presence of the "claw sign," defined as well-marginated linear regions of high signal located within the adjacent vertebral bodies at the interface of normal-abnormal marrow, was shown to be highly suggestive of Modic type 1 degenerative changes, with its absence suggesting infection.[48] However, in practice, morphological assessment on fat- and fluid-sensitive sequences, in addition to contrast-enhanced sequences if needed, is sufficient in most cases, and the added value of the claw sign in equivocal cases remains to be determined.

ADC values of infectious bone marrow are significantly higher than normal and degenerative bone marrow, and DWI has been proposed as an adjunct to conventional MRI to

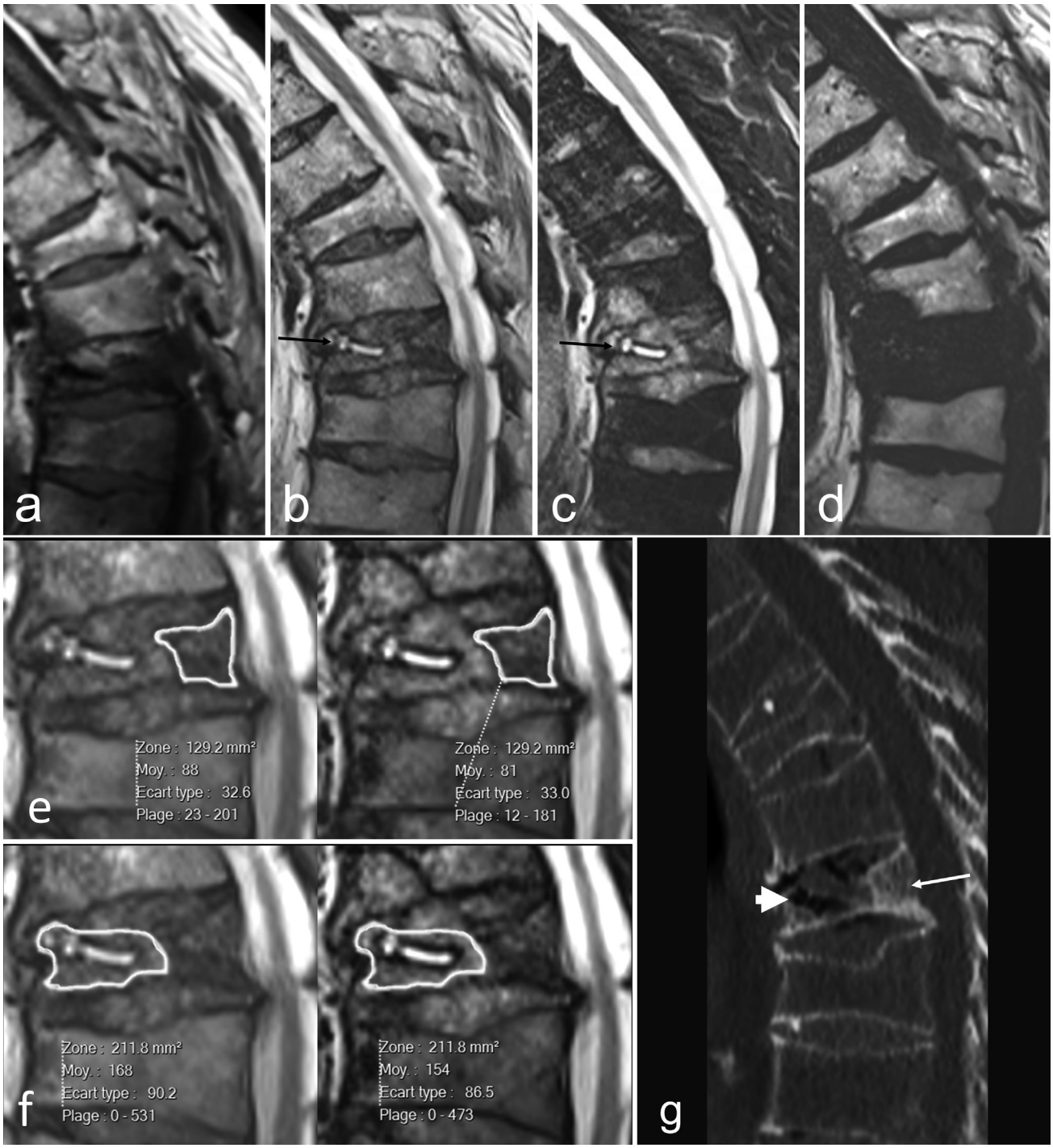

Fig. 3 An 82-year-old man with nontraumatic back pain. Sagittal (**a**) T1-weighted, (**b**) in-phase, (**c**) water-only, and (**d**) fat-onlyT2-weighted Dixon images show a recent vertebral compression fracture (VCF) of T12 with an intravertebral horizontal fluid-filled cleft (b, c, arrow) in favor of a benign VCF. However, the vertebral body did not show any residual fat (d), and there was no signal drop on out-of-phase images (**e**), suggestive of a marrow-replacing lesion. In view of the discordance, a vertebral biopsy was performed (not shown) that was negative for malignancy. (**g**) Sagittal reformat of computed tomography (CT) images show sclerotic changes in the posterior third of the vertebral body (arrow) and gas-containing cleft (arrowhead) as sources of false-positive findings on quantitative analysis of Dixon imaging. Follow-up fluorodeoxyglucose positron emission tomography/CT was negative for malignancy (not shown). Of importance, regions of interest should exclude fluid-filled regions to avoid false-positive results (**f**).

detect spinal infections especially if intravenous contrast injection is contraindicated[49–51] (►**Fig. 5**). The applicability of thresholds, however, is difficult in practice. The usefulness of ADC values in differentiating malignancy from infection was not consistently demonstrated across studies.[50,52,53]

Spondyloarthropathy

Few studies have assessed DWI to evaluate sacroiliitis, mostly showing inferiority to STIR images, limited added value to diagnose sacroiliitis, limited specificity, and poor interobserver agreement.[54–56] In one study, ADC values of

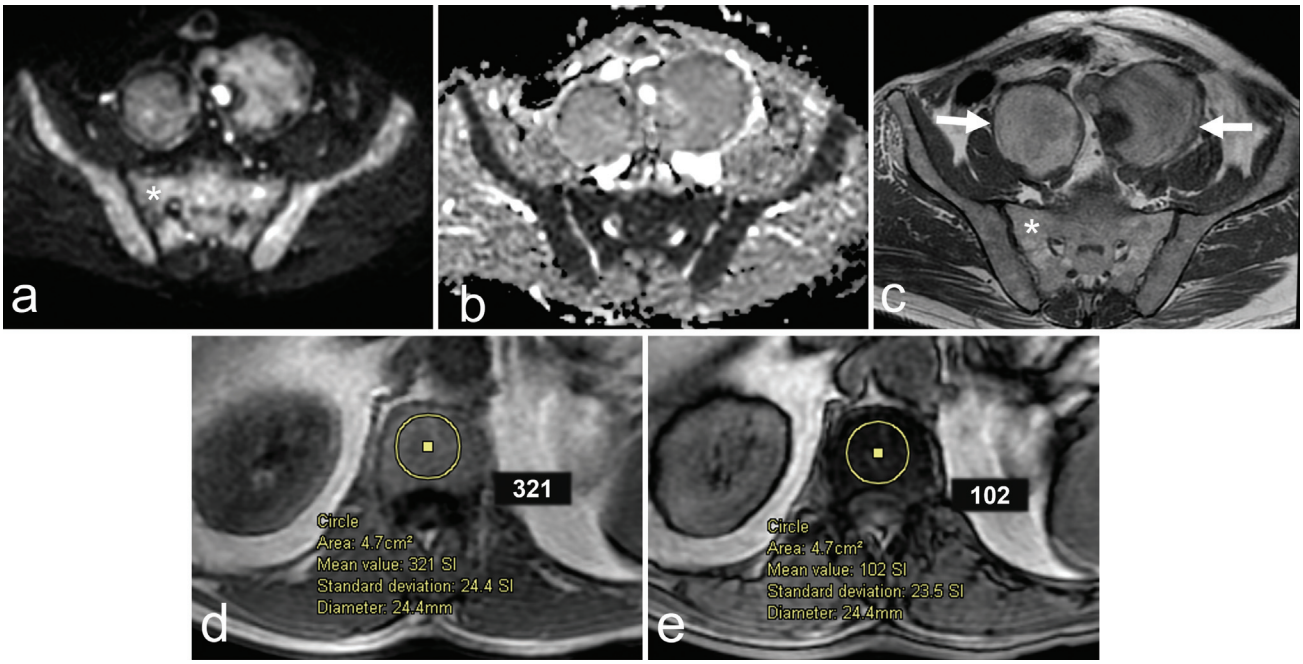

Fig. 4 A 65-year-old man with newly diagnosed rectal cancer referred for staging by magnetic resonance imaging (MRI) of the abdomen and pelvis. Transverse (**a**) diffusion-weighted image (DWI) (b = 600) and (**b**) corresponding apparent diffusion coefficient (ADC) map and (**c**) T1-weighted images show a diffuse increased signal of the marrow on DWI (a, asterisk) with restricted diffusion (ADC value: 0.62×10^{-3} mm^2/s) and normal T1 (c, asterisk). Known aneurysms of the iliac arteries treated by endovascular treatment (arrows). Transverse T1-weighted gradient-echo (**d**) in-phase and (**e**) out-of-phase images performed in the routine protocol of the abdomen show a 68% signal drop, indicating residual fat in keeping with marrow hyperplasia. The patient had severe anemia (Hb: 6.1 mg/dL).

edematous changes of vertebral endplate of rheumatologic origin were higher than those in Modic type 1 changes.[57]

Osteonecrosis

The T2-blackout effect on DWI (low DWI, low ADC) was described as a sign of early bone infarct and sequestration in a patient with sickle-cell disease.[58] However, DWI has limited value in the staging of femoral head osteonecrosis in clinical practice.[30,59]

Pitfalls

DWI encompasses a spectrum of sequences heavily influenced by technical parameters and patient-related factors. First, substantial technical variability exists among different

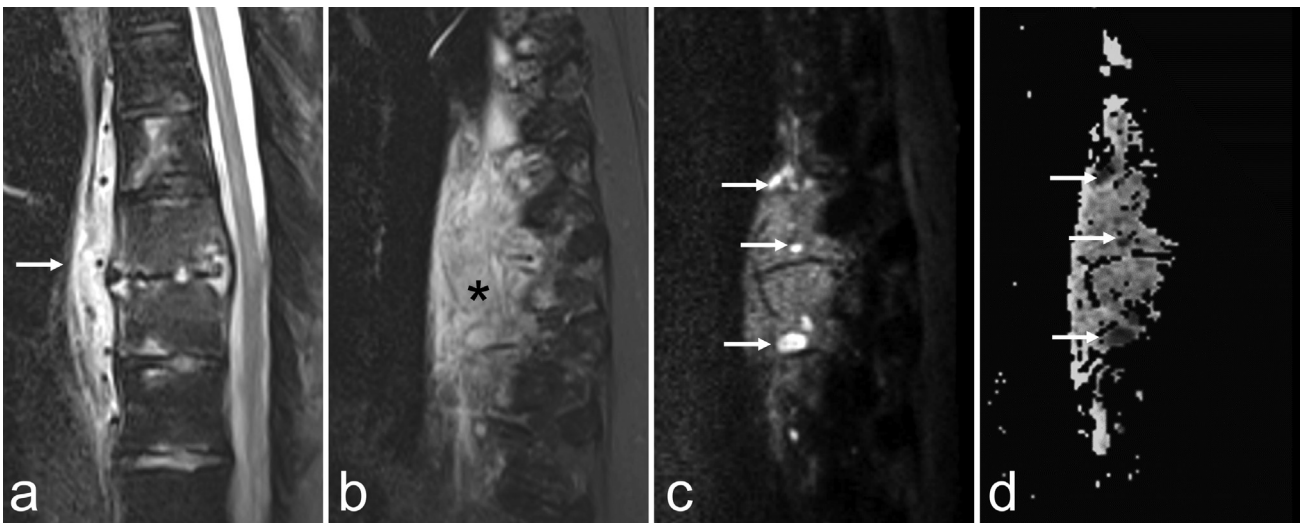

Fig. 5 A 29-year-old man with pyogenic spondylodiskitis. (**a**) Sagittal fat-suppressed T2-weighted image shows T8–T9 spondylodiskitis with a spread of the infection to the prevertebral soft tissues (arrow). Sagittal left paramedian (**b**) fat-suppressed T2-weighted diffusion-weighted image (DWI) (b = 700) and apparent diffusion coefficient map show a phlegmon involving the paravertebral soft tissues (asterisk) with areas of restricted diffusion (**c, d,** arrows) corresponding to (micro)abscesses. DWI can be useful to detect soft tissue abscesses if intravenous contrast injection is contraindicated.

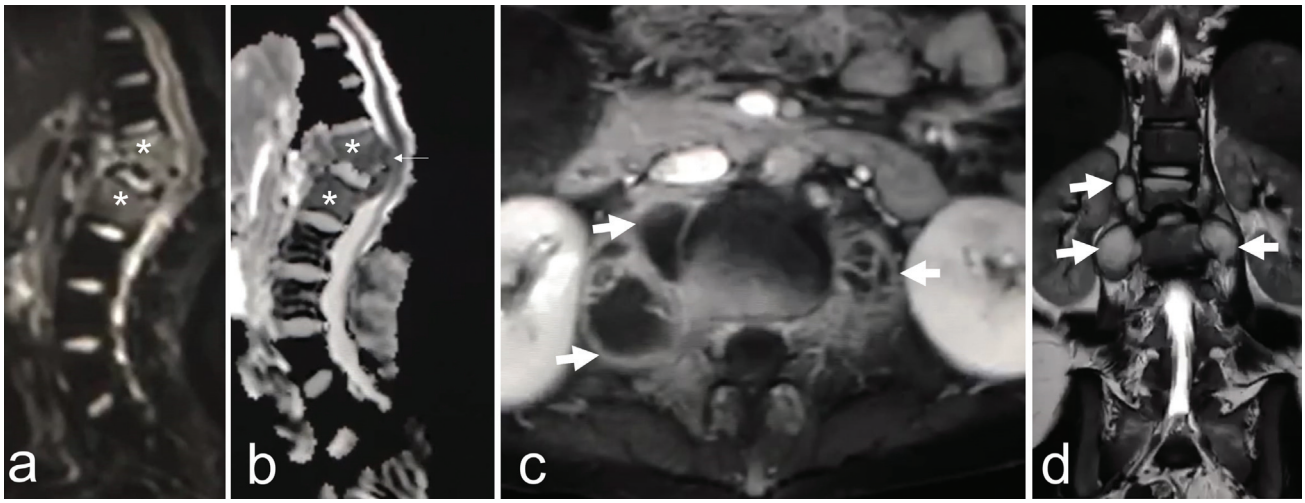

Fig. 6 A 12-year-old girl with painless progressive kyphosis. Sagittal (**a**) diffusion-weighted image (DWI) (b = 500) and (**b**) corresponding apparent diffusion coefficient (ADC) map, (**c**) transverse contrast-enhanced fat-suppressed T1-weighted images, and (**d**) coronal T2-weighted images show abnormal restricted diffusion of T12 and L1 vertebrae (asterisks) with epidural extension (b, arrow) and paravertebral peripherally enhancing collections with low T2 rim (c, d, arrows). The patient was found to have tuberculous spondylitis. The usefulness of ADC values in differentiating malignancy from infection is not consistent (courtesy of Joseph El-Khalil, MD, Beyrouth, Lebanon).

vendors and different institutions (e.g., EPI or FSE technique, field strength, fat suppression, choice of b-values).[34,35] Second, DWI is influenced by patient-related factors, whether physiologic (e.g., marrow composition, age, sex) or pathologic (e.g., anemia, osteoporosis)[60] (►**Fig. 4**). Third, the most widely used DWI techniques are EPI based that are prone to susceptibility artifacts at tissue boundaries (bone, lungs), more pronounced at higher field imaging, and a source of pitfalls in image interpretation.[61] For example, sclerotic metastases may alter image contrast on DWI, and blood products and metal debris may give erroneous ADC values in a postoperative setting.[51] Finally, due to the technical factors and lack of standardization, quantitative measurements have limited reproducibility, and there is frequently substantial overlap between cut-off values, hindering their universal applicability (►**Figs. 6** and **7**). Finally, the added value of DWI in comparison with conventional morphological imaging is yet to be determined.

Marrow Perfusion: Dynamic Contrast-enhanced MRI

Technique

DCE-MRI consists of assessing tissue perfusion through serial acquisitions of images before and after a bolus of intravenous contrast injection and the assessment of the variation of MR signal intensity of the tissues of interest, both qualitatively and quantitatively.

The nonmodeled quantitative and visual assessments in DCE-MRI are easily implemented in clinical settings and not computationally demanding. Images can be visually analyzed and regions of interest drawn on an area of interest to obtain DCE time-intensity curves. Qualitative assessment of contrast uptake, wash-in, and washout rates is the most widespread method in clinical routine.

The quantitative analysis is based on the Tofts bicompartmental model.[62,63] This quantitative analysis involves the conversion of signal intensity to gadolinium concentration and fitting of the data into a tissue model, and yields four main parameters (volume transfer constant [K^{trans}], rate constant [K_{ep}], fractional plasma volume [$V_{p,}$], and extravascular space [V_e]) that reflect the gadolinium distribution between the intravascular and the extravascular-extracellular compartment.[42] Quantitative DCE-MRI has been mainly used in a research setting to gain knowledge of the pathophysiology of various diseases such as osteoporosis, osteonecrosis, and osteoarthritis.[25,64,65]

Normal Bone Marrow

Normal bone marrow shows variable enhancement after intravenous contrast injection (mean: 20%; range: 3–59%).[66] However, vascularity depends on marrow composition, and red marrow is highly vascularized compared with yellow marrow.[16,67,68] Therefore, bone marrow perfusion on MRI may vary depending on marrow composition, age, and sex, with higher levels in women and decreasing levels with age.[66,69–71] The interpretation of DCE-MRI studies should be performed considering these physiologic differences.

Clinical Applications

Lesion Characterization and Evaluation of Vertebral Compression Fractures

Among the potential applications of DCE-MRI, it was suggested that the V_p, a quantitative parameter extracted from DCE-MRI, could differentiate benign from malignant VCFs with a sensitivity of 93% but a specificity of 78%.[72] Pathologic VCFs were shown to have higher perfusion parameters (V_p, K^{trans}, wash-in slope, peak enhancement, and area under the curve) compared with benign fractures.[73] However, the

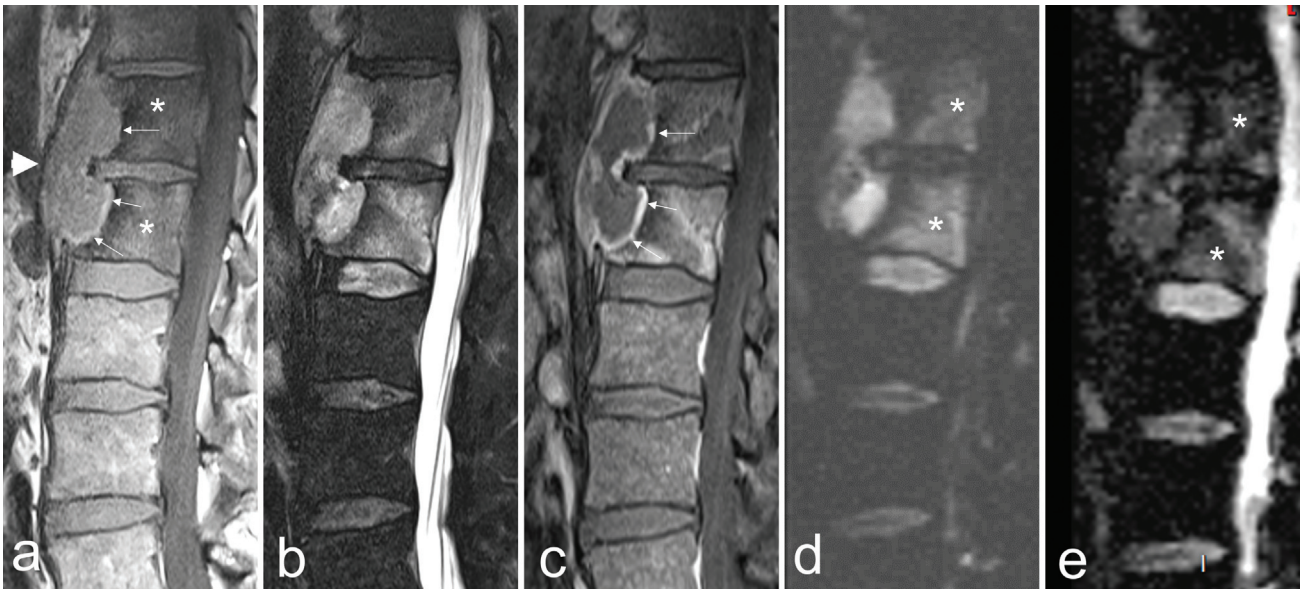

Fig. 7 A 53-year-old man with fever and back pain and suspicion of spondylodiskitis on computed tomography (CT) (not shown). Sagittal (**a**) T1-weighted, (**b**) fat-suppressed T2-weighted, (**c**) contrast-enhanced T1-weighted, (**d**) diffusion-weighted image (DWI) (b = 500), and (**e**) corresponding apparent diffusion coefficient (ADC) map show marrow replacement of T2 and L1 vertebral bodies, restricted DWI (asterisks) with an ADC value of 0.58 $\times 10^{-3}$ mm^2/s, a peripherally enhancing prevertebral collection with restricted DWI, causing scalloping of the anterior vertebral wall (thin arrows) and elevation without disruption of the anterior longitudinal ligament (a, arrowhead). The differential diagnosis included tuberculous spondylitis and lymphoma. The patient was diagnosed with Hodgkin's lymphoma on biopsy and positron emission tomography/computed tomography (not shown). There is an overlap of ADC values between malignant and infectious lesions, making the differentiation difficult based on quantitative imaging alone.

added value of DCE-MRI in cases where morphological analysis is inconclusive remains to be determined.

Diabetic Foot

DCE-MRI could be a useful adjunct to standard MRI protocols to help differentiate acute neuroarthropathy from pedal osteomyelitis. In one study, the K^{trans}, K^{ep}, and V_e values of bones with osteomyelitis were higher than those of acute neuropathic arthropathy.[74] In another study, the K^{trans} allowed a reliable differentiation between both entities but was inferior to the visual assessment of fluorodeoxyglucose positron emission tomography (FDG-PET)/CT.[47] DCE-MRI has also been used to predict and monitor treatment response in acute Charcot's foot.[75]

Spinal Infections

Quantitative analysis of DCE-MRI was shown to contribute to the early diagnosis of brucella spondylitis[76] and the differential diagnosis between spinal metastatic tumor, brucella spondylitis, and spinal tuberculosis.[76,77] Tuberculous vertebral lesions, especially in the early phases, may mimic malignant lesions on conventional MRI sequences but also on DWI (►**Figs. 6** and **7**). DCE-MRI has been used to assess spinal tuberculosis. On quantitative analysis, the presence of washout or a $K_{ep} \geq 1.17\,min^{-1}$ was shown to be highly predictive of malignancy.[78,79]

Pitfalls

Significant variations in imaging protocols, scanner types, and postprocessing methods hamper the universal applicability and reproducibility of quantitative DCE-MRI parameters. For example, quantitative parameters may vary depending on the acquisition protocols (amount of contrast agent, temporal resolution, and scan duration).[80]

Whole-body MR Imaging for Non-neoplastic Marrow Conditions: Applications and Challenges

Whole-body MRI has emerged as a useful tool in oncologic imaging (e.g., for staging, assessing disease burden, and treatment response). MRI acquisition protocols vary, but experts agree it should include T1-weighted, STIR, and DWI sequences, with recent trends toward using T2-weighted Dixon images to replace T1-weighted and STIR.[8,9,41,81]

Non-oncologic applications of whole-body MRI include the investigation of fever of unknown origin (FUO) in children,[82,83] the diagnosis and assessment of disease activity and treatment response in chronic recurrent multifocal osteomyelitis,[84–89] and synovitis, acne, pustulosis, hyperostosis, osteitis (SAPHO).[90] Whole-body MRI has also been used to detect clinically occult inflammatory lesions and to provide a simultaneous evaluation of the axial and appendicular skeleton in inflammatory arthritis.[91–98] Other applications include the evaluation of the disease burden in Gaucher's disease[99] and multifocal osteonecrosis.[100]

However, the incorporation of whole-body MRI into the routine clinical workflow remains challenging because of examination duration, the need for an experienced reader, and, in many countries, potential billing difficulties.[41] The

use of gradient-echo techniques, FSE T2-weighted Dixon sequences, and acceleration techniques, such as simultaneous multislice sequences and potentially reconstruction algorithms based on artificial intelligence, may contribute to decreasing acquisition time and allow wider use.[101,102]

Other Techniques of Marrow Imaging Using MRI

^{1}H-MRS spectroscopy provides concentrations of specific metabolites, and its main application in marrow imaging is the quantification of fat.[36,103] In clinical research, it has been investigated in a few applications related to osteoporosis, fracture risk assessment, and response to treatment in patients with metabolic diseases like anorexia nervosa,[104,105] Gaucher's disease,[106] rheumatoid arthritis,[107] multiple myeloma,[108] or Charcot's neuroarthropathy.[109] However, in clinical practice, its use has significantly decreased in favor of CSI.[110]

Intravoxel incoherent motion MRI uses low b-value DWI to acquire perfusion maps without the need for contrast injection. This technique has been applied in neuroradiology and oncology, and it may be used to assess muscle perfusion. However, its usefulness in marrow imaging in clinical practice remains to be validated by further studies.[111,112]

Spectral Computed Tomography Imaging

Technique

Spectral CT is based on the principle that the attenuation of tissues depends not only on their density but also on their atomic number Z, as well as on the energy of the photon beam.[113] Using these properties, spectral CT may be used to characterize and quantify certain tissue components. As an example, mineralized tissues of bones can be subtracted from the image and VNCa images may be obtained, allowing the detection of bone marrow lesions.[114,115]

The most commonly available subset of spectral CT is DECT, in which two X-ray energy spectra are used. More recently, photon counting detectors were introduced. This new technology allows multi-energy imaging, a direct count of individual incoming photons, and a measure of their energy level.[116,117] Photon counting detectors can provide higher spatial resolution, dose reduction, and better material differentiation, and they are less prone to beam-hardening artifacts.[116–118] The following sections summarize some applications of DECT for bone marrow imaging, keeping in mind that photon counting CT has the potential to improve the diagnostic performance of DECT for these applications, although this is yet to be validated.

Normal Bone Marrow

DECT may be used to assess bone marrow composition.[119] However, to the best of our knowledge, no consensus has been reached on the definition of normal bone marrow on DECT. In fact, image analysis is based on a comparison of areas of interest with the presumed normal bone marrow within the FOV and is influenced by postprocessing algorithms and thresholding parameters.

Clinical Applications

Detection of Bone Marrow Edema and Marrow-replacing Lesions

The performance of conventional CT to detect bone marrow lesions that do not alter the mineralized bone is poor. VNCa reconstructions have the potential to improve the detection of BME-like lesions, as well as bone marrow–replacing lesions. For sake of simplicity, we use "BME" to refer to BME-like lesions in the rest of this section.

The DECT depiction of BME most commonly uses two material decomposition algorithms (calcium/water) based on different attenuation profiles at different energies. VNCa images can hereby be generated, allowing the assessment of bone marrow attenuation. VNCa images are often interpreted as color maps coding the attenuation of bone marrow and may be fused with native bone images for better anatomical correlations.[120]

Bone marrow neoplastic lesions, unless lytic or sclerotic, are difficult to detect on conventional CT. VNCa images were shown potentially useful for the detection of bone marrow lesions in multiple myeloma[121] and metastases of solid tumors.[122]

Moreover, studies have used DECT to differentiate malignant from nonmalignant tumors,[123] osteoblastic metastases from bone islands,[124] osteolytic metastases from Schmorl's nodes,[125] and infections.[126] However, MRI so far remains the keystone morphological modality for imaging bone marrow, and more validation studies of DECT are required.

Vertebral Compression Fractures

DECT allows the detection of BME and the differentiation of acute from chronic VCFs.[120,127–131] In a recent systematic review and meta-analysis, DECT had 89% sensitivity and 96% specificity to diagnose BME related to a recent VCF, possibly obviating the need for a confirmatory MRI in the emergency setting.[132] However, CT with a single-source technique had poorer specificity (78%) compared with those with a dual-source technique (98%), the diagnostic accuracy for the detection of BME depended on the reader's experience, and the absence of BME did not confidently rule out the diagnosis of acute VCF if the clinical suspicion was high.[132] Of importance, the sensitivity of DECT in the diagnosis of acute but morphologically occult VCFs remains to be addressed.[132]

Trauma of the Appendicular Skeleton

In clinical practice, CT is used in traumatic contexts with noncontributory radiographs and clinical suspicion of fracture. However, the lack of cortical discontinuity or trabecular displacement can make the diagnosis challenging. MRI is considered the gold standard for detecting BME in occult fractures; however, it is not widely available in the emergency context.

VNCa images may improve visualization of occult fractures and improve the reliability and diagnostic confidence among less experienced readers.[120,133] In a recent meta-analysis, DECT had a pooled sensitivity and specificity of 86% and 93%, respectively.[134] DECT reduces the reading time

while analyzing lower extremity CTs for fractures when the radiologist is presented with BME maps, and time reductions were more evident for unskilled readers.[135] DECT could potentially function as a one-stop shop and obviate the need for confirmatory MRI.

Low-energy Trauma of Older Adults

DECT increases the sensitivity to detect radiographically occult fractures of the pelvic girdle and proximal femurs in older adults, whether related to low-energy trauma or bone insufficiency.[136–140] Some authors have suggested that a quantitative analysis of VNCa images might help differentiate pathologic from nonpathologic fractures.[141] However, this finding should be confirmed in larger studies.

Rheumatologic Disorders

DECT can detect inflammatory lesions in sacroiliitis with relatively high sensitivities (between 81% and 93%) and specificities (91–94%).[142,143] The incidental detection of periarticular BME may help in the early diagnosis of rheumatologic disorders.[120]

Miscellaneous Marrow Conditions

DECT can detect nontraumatic BME of the hip and knee with a sensitivity of 88.4% and specificity of 96.1%.[144] If MRI is contraindicated, DECT could help depict BME associated with cortical erosions confirming osteomyelitis. This possibility should be validated in further studies.[120]

Pitfalls and Limitations

Validation of established diagnostic thresholds for bone marrow alterations is difficult because of the variety of acquisition and postprocessing methods[132,145,146] (►**Fig. 8**). The ability of the material decomposition in DECT increases with lower spectral overlap.[147] Therefore, a wider separation between the energies of the two tubes could improve DECT sensitivity to detect BME.[148]

As a general recommendation, VNCa maps should not be assessed in isolation, and the reader must be aware of possible pitfalls. Any process that locally increases the attenuation of the bone marrow to a density higher than fat could show false-positive results. Red marrow hyperplasia can be misinterpreted as BME (i.e., in the proximal femurs and flat bones as vertebrae). Hence careful comparison with the contralateral side and adjacent structures is recommended when looking for an occult fracture.

Bone sclerosis can cause both false-positive findings due to locally increased Hounsfield unit levels, and false-negative findings as an extensive subtraction process can hide BME detection. In the presence of a splint or cast, BME may not show even in displaced fractures, probably due to a reduction in the attenuation differences caused by the dense material around the limb.[120] In general, VNCa maps should always be assessed together with conventional images to avoid pitfalls.

Additional limitations related to technical challenges, standardization of reconstruction, and decomposition algorithms, as well as window level and width settings, remain to be addressed before the widespread implementation of DECT in marrow imaging.

Nuclear Medicine and Molecular Imaging

Technique

Nuclear imaging relies on the intravenous injection of radiopharmaceuticals to assess the distribution of hematopoietic or reticuloendothelial cells. Imaging of the hematopoietic component can be achieved by white blood cell (WBC) scintigraphy, by injecting the patient's WBCs after they have been radiolabeled in vitro with technetium (Tc)-99m (Tc) or indium-111, or by injecting Tc-99m-labeled mouse anti-granulocytes monoclonal antibodies or antibody fragments. The reticuloendothelial cells may be imaged thanks to radiolabeled colloids (Tc-99m-sulfur colloid

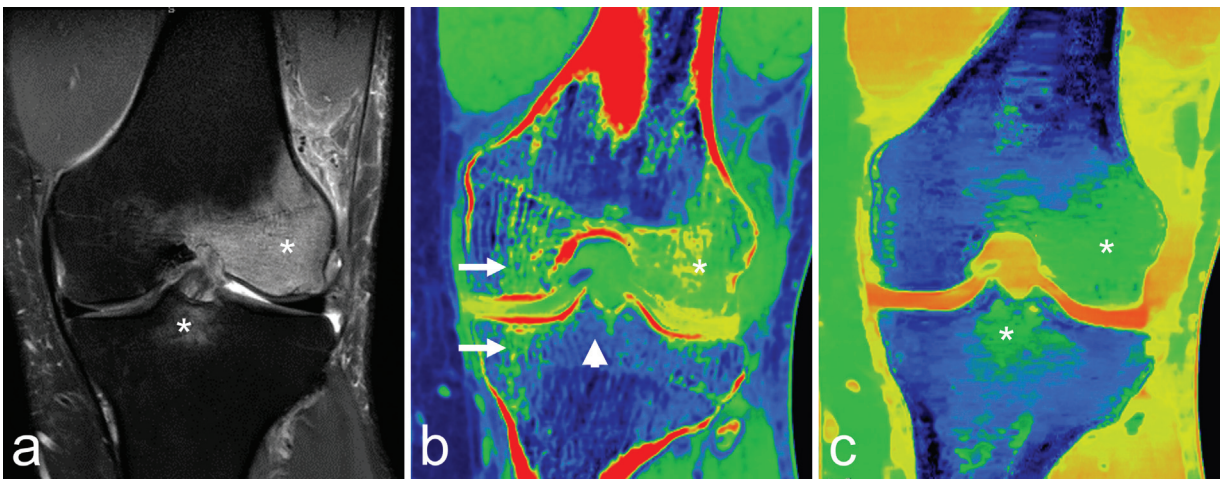

Fig. 8 A 46-year-old man with left knee pain. (**a**) Coronal intermediate-weighted fat-suppressed image shows edema-like signal intensity of the lateral femoral condyle and the tibial eminence (asterisks). Two types of coronal color-coded dual-energy computed tomography reconstructions are displayed: (**b**) virtual non-calcium and (**c**) virtual non-hydroxyapatite, showing the influence of postprocessing. There are false positives (arrows) and false negatives (arrowhead) (b).

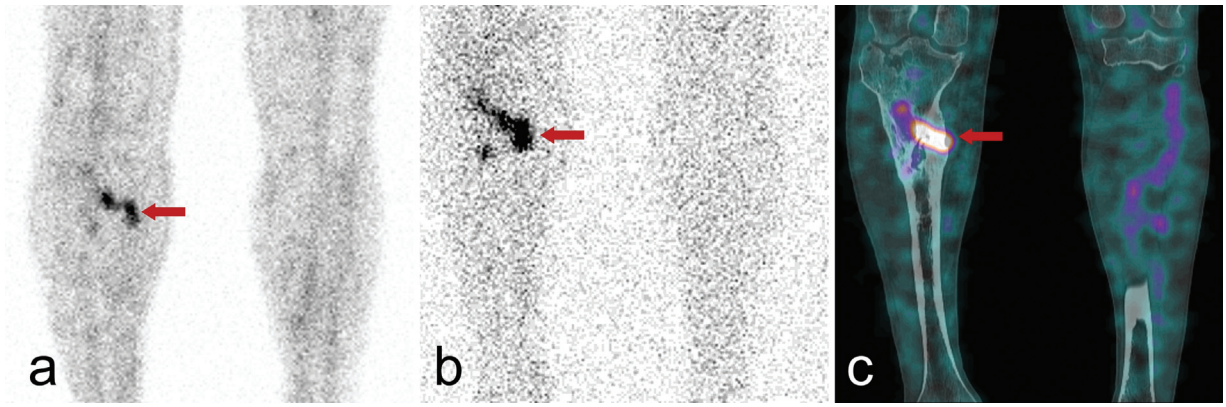

Fig. 9 A 54-year-old man with a history of previous right tibial fracture and suspicion of osteomyelitis. Anterior planar images were acquired at (**a**) 4 hours and (**b**) 24 hours after intravenous injection of mouse monoclonal 99m-technetium-antigranulocyte antibodies showing focal accumulation of leukocytes in the right tibial diaphysis (arrow). (**c**) Coronal fused single-photon emission computed tomography/computed tomography images confirmed that the uptake corresponds to the site of the previous tibial fracture (arrow).

and Tc-99m-nanocolloid) that are phagocytosed by the reticuloendothelial system in bone marrow, spleen, and liver. Bone scintigraphy with intravenous injection of Tc-99m-labeled diphosphonates allows imaging of bone osteoblastic activity.

Furthermore, the metabolic activity of bone marrow can be probed by ^{18}F-Fluoro-deoxyglucose positron emission tomography (^{18}FDG PET).

Osteomyelitis

WBC scintigraphy has high accuracy in evaluating infections involving the appendicular skeleton. However, its diagnostic performance for the detection of infection in the axial skeleton is hampered by intense physiologic bone marrow uptake.

^{18}FDG PET/CT may be used in patients in whom MRI is contraindicated to detect sites of infection in the axial skeleton (i.e., spondylodiscitis). Focal FDG uptake in the diabetic foot may be a useful sign to differentiate osteomyelitis from Charcot's neuro-osteoarthropathy when MRI is inconclusive.[47] In a 2017 meta-analysis, WBC scintigraphy and FDG-PET had a comparable sensitivity to MRI but a higher specificity to diagnose pedal osteomyelitis.[149] In addition, WBC scintigraphy has high diagnostic accuracy to evaluate fracture-related infections[150] (►**Fig. 9**).

WBC imaging is also a valuable tool to assess periprosthetic infections. Bone scintigraphy is highly sensitive but not specific for septic loosening, whereas WBC scintigraphy has high sensitivity and specificity for infection.[151–153] In practice, the absence of periprosthetic uptake on bone scan practically rules out infection, whereas an increased periprosthetic uptake should be complemented by WBC scintigraphy, with or without a colloid scan.[153]

In cases of FUO, FDGPET has higher diagnostic accuracy than WBC scintigraphy to detect the infectious site, although the latter is more specific.[152,154,155] A new technique consisting of radiolabeling WBC with FDG might replace Tc-99m WBC in this setting because it is more specific than FDG-PET/CT and more sensitive than WBC scintigraphy.[156]

Vertebral Compression Fractures and Occult Fractures

Bone scintigraphy can depict VCFs because it is a very sensitive method for detecting active bone remodeling.[157] In patients with MRI contraindications and multiple vertebral fractures, it may help guide therapy by pointing out the most recent fracture. Bone scintigraphy is also an excellent imaging alternative to MRI in patients with suspicion of occult fractures.[158]

Focal Marrow Hypermetabolism on FDG-PET/CT

Normal bone marrow metabolism is variable and declines with age.[159] Diffuse increase in bone marrow metabolism can occur in hematologic malignancies but is frequently observed in non-neoplastic conditions resulting in marrow stimulation such as sepsis, rebound hematopoiesis after chemotherapy, or following the administration of hematopoietic growth factors.[160,161] A focal FDG uptake may be due to infection or focal medullary hyperplasia that may mimic metastatic lesions in an oncologic setting.[19] In cases where the characterization of a single uptake is crucial for staging (i.e., no other metastases), MRI with CSI may be useful (►**Fig. 1**).

Miscellaneous Applications

WBC and, to a lower degree, colloid scintigraphy can be used for the diagnosis of extramedullary hematopoiesis.[162] In addition, WBC scintigraphy can also be used to map bone marrow in cancer patients with impaired bone marrow function to help predict the effect of therapies such as external radiotherapy or metabolic radiotherapy on hematopoiesis[163] (►**Fig. 10**).

Limitations and Pitfalls

Nuclear imaging techniques present some general limitations including the need for a specific technical platform (WBC scintigraphy), the radiation dose, and cost-related issues.

Pitfalls exist and vary according to the radiotracer used. An extensive review of these pitfalls is beyond the scope of

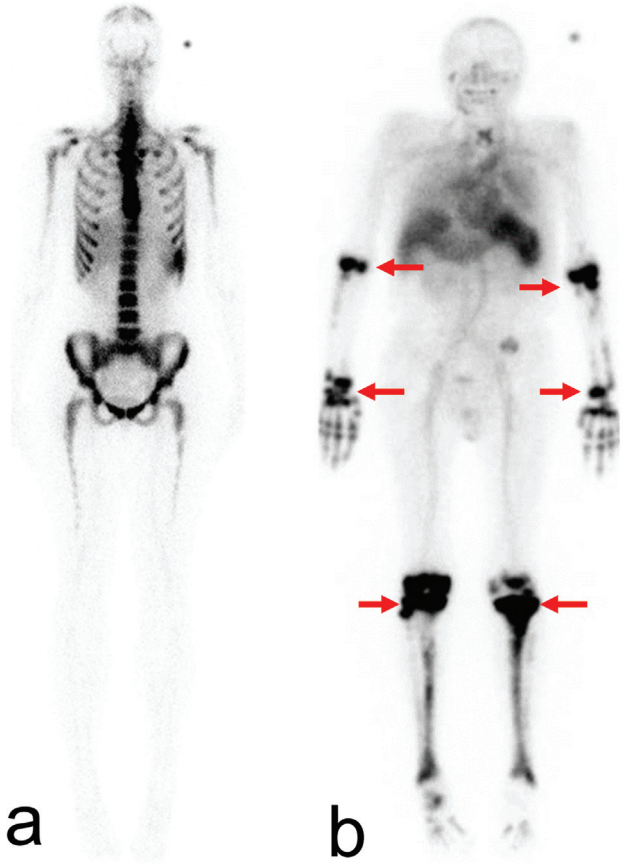

Fig. 10 (**a**) Anterior planar image of the whole body acquired 4 hours after intravenous injection of mouse monoclonal 99m-technetium (Tc)-antigranulocyte antibodies showing a normal distribution pattern of the radiotracer in a 37-year-old patient. Note the distribution of the radiotracer in the axial skeleton and the absence of uptake in the appendicular skeleton, paralleling the normal red marrow distribution in adults. (**b**) Anterior planar image of the whole body acquired 4 hours after intravenous injection of mouse monoclonal 99m-Tc-antigranulocyte antibodies in a 75-year-old man with metastatic prostate cancer, showing an intense abnormal uptake in the appendicular skeleton (arrows), together with the absence of uptake in the axial skeleton as compared with the normal pattern in (a). Bone marrow hyperplasia in the peripheral skeleton has occurred as a consequence of diffuse marrow replacement by metastases in the axial skeleton.

this article, but a good understanding of the physiology and distribution of each radiotracer is essential to avoid several of these pitfalls, including false-positive findings.

Conclusion

Over the past decades, there has been a growing interst in novel imaging techniques for the assessment of bone marrow, both qualitatively and quantitatively. Although many of these methods have been successfully used in the research setting, their incorporation in clinical practice has been limited. Many challenges remain to be addressed, including availability, cross-vendor and cross-institutional reproducibility, issues related to reimbursement, as well as examination and processing time. Once these challenges are overcome and techniques are standardized, further studies will be needed to assess the added value of these methods in relation to conventional protocols.

Conflict of Interest
None declared.

Acknowlegment
The authors would like to thank Jean-Baptiste Ledoux for his help in producing high quality images.

References

1 Geith T, Schmidt G, Biffar A, et al. Comparison of qualitative and quantitative evaluation of diffusion-weighted MRI and chemical-shift imaging in the differentiation of benign and malignant vertebral body fractures. AJR Am J Roentgenol 2012;199(05): 1083–1092
2 Zajick DC Jr, Morrison WB, Schweitzer ME, Parellada JA, Carrino JA. Benign and malignant processes: normal values and differentiation with chemical shift MR imaging in vertebral marrow. Radiology 2005;237(02):590–596
3 Schmeel FC, Luetkens JA, Wagenhäuser PJ, et al. Proton density fat fraction (PDFF) MRI for differentiation of benign and malignant vertebral lesions. Eur Radiol 2018;28(06):2397–2405
4 Colombo A, Bombelli L, Summers PE, et al. Effects of sex and age on fat fraction, diffusion-weighted image signal intensity and apparent diffusion coefficient in the bone marrow of asymptomatic individuals: a cross-sectional whole-body MRI study. Diagnostics (Basel) 2021;11(05):913
5 Kirchgesner T, Perlepe V, Michoux N, Larbi A, Vande Berg B. Fat suppression at 2D MR imaging of the hands: Dixon method versus CHESS technique and STIR sequence. Eur J Radiol 2017; 89:40–46
6 Ma J, Singh SK, Kumar AJ, Leeds NE, Zhan J. T2-weighted spine imaging with a fast three-point Dixon technique: comparison with chemical shift selective fat suppression. J Magn Reson Imaging 2004;20(06):1025–1029
7 Yang S, Lassalle L, Mekki A, et al. Can T2-weighted Dixon fat-only images replace T1-weighted images in degenerative disc disease with Modic changes on lumbar spine MRI? Eur Radiol 2021;31 (12):9380–9389
8 Danner A, Brumpt E, Alilet M, Tio G, Omoumi P, Aubry S. Improved contrast for myeloma focal lesions with T2-weighted Dixon images compared to T1-weighted images. Diagn Interv Imaging 2019;100(09):513–519
9 Maeder Y, Dunet V, Richard R, Becce F, Omoumi P. Bone marrow metastases: T2-weighted Dixon spin-echo fat images can replace T1-weighted spin-echo images. Radiology 2018;286(03): 948–959
10 Zanchi F, Richard R, Hussami M, Monier A, Knebel JF, Omoumi P. MRI of non-specific low back pain and/or lumbar radiculopathy: do we need T1 when using a sagittal T2-weighted Dixon sequence? Eur Radiol 2020;30(05):2583–2593
11 Omoumi P. The Dixon method in musculoskeletal MRI: from fat-sensitive to fat-specific imaging. Skeletal Radiol 2022;51(07): 1365–1369
12 Hahn S, Lee YH, Suh JS. Detection of vertebral metastases: a comparison between the modified Dixon turbo spin echo T_2 weighted MRI and conventional T_1 weighted MRI: a preliminary study in a tertiary centre. Br J Radiol 2018;91(1085):20170782
13 Bacher S, Hajdu SD, Maeder Y, Dunet V, Hilbert T, Omoumi P. Differentiation between benign and malignant vertebral compression fractures using qualitative and quantitative analysis of a single fast spin echo T2-weighted Dixon sequence. Eur Radiol 2021;31(12):9418–9427

14 Omoumi P, Obuchowski NA. How to show that a new imaging method can replace a standard method, when no reference standard is available? Eur Radiol 2022;32(04):2810–2812
15 Carroll KW, Feller JF, Tirman PF. Useful internal standards for distinguishing infiltrative marrow pathology from hematopoietic marrow at MRI. J Magn Reson Imaging 1997;7(02):394–398
16 Vande Berg BC, Malghem J, Lecouvet FE, Maldague B. Magnetic resonance imaging of the normal bone marrow. Skeletal Radiol 1998;27(09):471–483
17 Vande Berg BC, Lecouvet FE, Galant C, Maldague BE, Malghem J. Normal variants and frequent marrow alterations that simulate bone marrow lesions at MR imaging. Radiol Clin North Am 2005; 43(04):761–770, ix
18 Kohl CA, Chivers FS, Lorans R, Roberts CC, Kransdorf MJ. Accuracy of chemical shift MR imaging in diagnosing indeterminate bone marrow lesions in the pelvis: review of a single institution's experience. Skeletal Radiol 2014;43(08):1079–1084
19 Rajakulasingam R, Saifuddin A. Focal nodular marrow hyperplasia: imaging features of 53 cases. Br J Radiol 2020;93 (1112):20200206
20 Ragab Y, Emad Y, Gheita T, et al. Differentiation of osteoporotic and neoplastic vertebral fractures by chemical shift in-phase and out-of phase MR imaging. Eur J Radiol 2009;72(01):125–133
21 Yoo HJ, Hong SH, Kim DH, et al. Measurement of fat content in vertebral marrow using a modified Dixon sequence to differentiate benign from malignant processes. J Magn Reson Imaging 2017;45(05):1534–1544
22 Kwack KS, Lee HD, Jeon SW, Lee HY, Park S. Comparison of proton density fat fraction, simultaneous R2*, and apparent diffusion coefficient for assessment of focal vertebral bone marrow lesions. Clin Radiol 2020;75(02):123–130
23 Özgen A. The value of the T2-weighted multipoint Dixon sequence in MRI of sacroiliac joints for the diagnosis of active and chronic sacroiliitis. AJR Am J Roentgenol 2017;208(03):603–608
24 Huang H, Zhang Y, Zhang H, et al. Qualitative and quantitative assessment of sacroiliitis in axial spondyloarthropathy: can a single T2-weighted Dixon sequence replace the standard protocol? Clin Radiol 2020;75(04):321.e13–321.e20
25 Griffith JF, Yeung DKW, Antonio GE, et al. Vertebral marrow fat content and diffusion and perfusion indexes in women with varying bone density: MR evaluation. Radiology 2006;241(03): 831–838
26 Wáng YXJ, Griffith JF, Deng M, Yeung DK, Yuan J. Rapid increase in marrow fat content and decrease in marrow perfusion in lumbar vertebra following bilateral oophorectomy: an MR imaging-based prospective longitudinal study. Korean J Radiol 2015;16 (01):154–159
27 Kühn JP, Hernando D, Meffert PJ, et al. Proton-density fat fraction and simultaneous R2* estimation as an MRI tool for assessment of osteoporosis. Eur Radiol 2013;23(12):3432–3439
28 You JH, Kim IH, Hwang J, Lee HS, Park EH. Fracture of ankle: MRI using opposed-phase imaging obtained from turbo spin echo modified Dixon image shows improved sensitivity. Br J Radiol 2018;91(1088):20170779
29 Saifuddin A, Santiago R, van Vucht N, Pressney I. Comparison of T1-weighted turbo spin echo and out-of-phase T1-weighted gradient echo Dixon MRI for the assessment of intra-medullary length of appendicular bone tumours. Skeletal Radiol 2021;50 (05):993–1005
30 Han X, Hong G, Guo Y, et al. Novel MRI technique for the quantification of biochemical deterioration in steroid-induced osteonecrosis of femoral head: a prospective diagnostic trial. J Hip Preserv Surg 2021;8(01):40–50
31 van Vucht N, Santiago R, Pressney I, Saifuddin A. Anomalous signal intensity increase on out-of-phase chemical shift imaging: a manifestation of marrow mineralisation? Skeletal Radiol 2020; 49(08):1269–1275
32 Takasu M, Kaichi Y, Tani C, et al. Iterative decomposition of water and fat with echo asymmetry and least-squares estimation (IDEAL) magnetic resonance imaging as a biomarker for symptomatic multiple myeloma. PLoS One 2015;10(02):e0116842
33 Borga M, Ahlgren A, Romu T, Widholm P, Dahlqvist Leinhard O, West J. Reproducibility and repeatability of MRI-based body composition analysis. Magn Reson Med 2020;84(06):3146–3156
34 Biffar A, Dietrich O, Sourbron S, Duerr HR, Reiser MF, Baur-Melnyk A. Diffusion and perfusion imaging of bone marrow. Eur J Radiol 2010;76(03):323–328
35 Dietrich O, Geith T, Reiser MF, Baur-Melnyk A. Diffusion imaging of the vertebral bone marrow. NMR Biomed 2017;30(03):e3333
36 Karampinos DC, Ruschke S, Dieckmeyer M, et al. Quantitative MRI and spectroscopy of bone marrow. J Magn Reson Imaging 2018;47(02):332–353
37 Kruk KA, Dietrich TJ, Wildermuth S, et al. Diffusion-weighted imaging distinguishes between osteomyelitis, bone marrow edema, and healthy bone on forefoot magnetic resonance imaging. J Magn Reson Imaging 2022;56(05):1571–1579
38 Dietrich O, Biffar A, Reiser MF, Baur-Melnyk A. Diffusion-weighted imaging of bone marrow. Semin Musculoskelet Radiol 2009; 13(02):134–144
39 Zhang CY, Rong R, Wang XY. Age-related changes of bone marrow of normal adult man on diffusion weighted imaging. Chin Med Sci J 2008;23(03):162–165
40 Tsujikawa T, Oikawa H, Tasaki T, et al. Whole-body bone marrow DWI correlates with age, anemia, and hematopoietic activity. Eur J Radiol 2019;118:223–230
41 Ahlawat S, Debs P, Amini B, Lecouvet FE, Omoumi P, Wessell DE. Clinical applications and controversies of whole-body MRI: *AJR* expert panel narrative review. AJR Am J Roentgenol 2022
42 Van Den Berghe T, Verstraete KL, Lecouvet FE, Lejoly M, Dutoit J. Review of diffusion-weighted imaging and dynamic contrast-enhanced MRI for multiple myeloma and its precursors (monoclonal gammopathy of undetermined significance and smouldering myeloma). Skeletal Radiol 2022;51(01):101–122
43 Messiou C, Hillengass J, Delorme S, et al. Guidelines for acquisition, interpretation, and reporting of whole-body MRI in myeloma: Myeloma Response Assessment and Diagnosis System (MY-RADS). Radiology 2019;291(01):5–13
44 Suh CH, Yun SJ, Jin W, Lee SH, Park SY, Ryu CW. ADC as a useful diagnostic tool for differentiating benign and malignant vertebral bone marrow lesions and compression fractures: a systematic review and meta-analysis. Eur Radiol 2018;28(07):2890–2902
45 Eren MA, Karakaş E, Torun AN, Sabuncu T. The clinical value of diffusion-weighted magnetic resonance imaging in diabetic foot infection. J Am Podiatr Med Assoc 2019;109(04):277–281
46 Abdel Razek AAK, Samir S. Diagnostic performance of diffusion-weighted MR imaging in differentiation of diabetic osteoarthropathy and osteomyelitis in diabetic foot. Eur J Radiol 2017; 89:221–225
47 Diez AIG, Fuster D, Morata L, et al. Comparison of the diagnostic accuracy of diffusion-weighted and dynamic contrast-enhanced MRI with ^{18}F-FDG PET/CT to differentiate osteomyelitis from Charcot neuro-osteoarthropathy in diabetic foot. Eur J Radiol 2020;132:109299
48 Patel KB, Poplawski MM, Pawha PS, Naidich TP, Tanenbaum LN. Diffusion-weighted MRI "claw sign" improves differentiation of infectious from degenerative modic type 1 signal changes of the spine. AJNR Am J Neuroradiol 2014;35(08):1647–1652
49 Eguchi Y, Ohtori S, Yamashita M, et al. Diffusion magnetic resonance imaging to differentiate degenerative from infectious endplate abnormalities in the lumbar spine. Spine 2011;36(03): E198–E202
50 Dumont RA, Keen NN, Bloomer CW, et al. Clinical utility of diffusion-weighted imaging in spinal infections. Clin Neuroradiol 2019;29(03):515–522

51 Moritani T, Kim J, Capizzano AA, Kirby P, Kademian J, Sato Y. Pyogenic and non-pyogenic spinal infections: emphasis on diffusion-weighted imaging for the detection of abscesses and pus collections. Br J Radiol 2014;87(1041):20140011

52 Balliu E, Vilanova JC, Peláez I, et al. Diagnostic value of apparent diffusion coefficients to differentiate benign from malignant vertebral bone marrow lesions. Eur J Radiol 2009;69(03):560–566

53 Pui MH, Mitha A, Rae WID, Corr P. Diffusion-weighted magnetic resonance imaging of spinal infection and malignancy. J Neuroimaging 2005;15(02):164–170

54 Kucybała I, Ciuk S, Urbanik A, Wojciechowski W. The usefulness of diffusion-weighted imaging (DWI) and dynamic contrast-enhanced (DCE) sequences visual assessment in the early diagnosis of axial spondyloarthritis. Rheumatol Int 2019;39(09): 1559–1565

55 Boy FN, Kayhan A, Karakas HM, Unlu-Ozkan F, Silte D, Aktas İ The role of multi-parametric MR imaging in the detection of early inflammatory sacroiliitis according to ASAS criteria. Eur J Radiol 2014;83(06):989–996

56 Chung HY, Xu X, Lau VWH, et al. Comparing diffusion weighted imaging with clinical and blood parameters, and with short tau inversion recovery sequence in detecting spinal and sacroiliac joint inflammation in axial spondyloarthritis. Clin Exp Rheumatol 2017;35(02):262–269

57 Dallaudière B, Dautry R, Preux PM, et al. Comparison of apparent diffusion coefficient in spondylarthritis axial active inflammatory lesions and type 1 Modic changes. Eur J Radiol 2014;83(02): 366–370

58 Tuna IS, Tarhan B, Escobar M, Albayram MS. T2-blackout effect on DWI as a sign of early bone infarct and sequestration in a patient with sickle cell disease. Clin Imaging 2019;54:15–20

59 Öner AY, Aggunlu L, Akpek S, et al. Staging of hip avascular necrosis: is there a need for DWI? Acta Radiol 2011;52(01): 111–114

60 Cui FZ, Yao QQ, Cui JL, Wei W, Duan LS, Yu H. The signal intensity characteristics of normal bone marrow in diffusion weighted imaging at various menstrual status women. Eur J Radiol 2021; 143:109938

61 Raya JG, Dietrich O, Reiser MF, Baur-Melnyk A. Techniques for diffusion-weighted imaging of bone marrow. Eur J Radiol 2005; 55(01):64–73

62 Leach MO, Morgan B, Tofts PS, et al; Experimental Cancer Medicine Centres Imaging Network Steering Committee. Imaging vascular function for early stage clinical trials using dynamic contrast-enhanced magnetic resonance imaging. Eur Radiol 2012;22(07):1451–1464

63 Tofts PS, Brix G, Buckley DL, et al. Estimating kinetic parameters from dynamic contrast-enhanced T(1)-weighted MRI of a diffusable tracer: standardized quantities and symbols. J Magn Reson Imaging 1999;10(03):223–232

64 Daugaard CL, Riis RG, Bandak E, et al. Perfusion in bone marrow lesions assessed on DCE-MRI and its association with pain in knee osteoarthritis: a cross-sectional study. Skeletal Radiol 2020;49(05):757–764

65 Cultot A, Norberciak L, Coursier R, et al. Bone perfusion and adiposity beyond the necrotic zone in femoral head osteonecrosis: a quantitative MRI study. Eur J Radiol 2020;131:109206

66 Baur A, Stäbler A, Bartl R, Lamerz R, Scheidler J, Reiser M. MRI gadolinium enhancement of bone marrow: age-related changes in normals and in diffuse neoplastic infiltration. Skeletal Radiol 1997;26(07):414–418

67 Weiss L. The structure of bone marrow. Functional interrelationships of vascular and hematopoietic compartments in experimental hemolytic anemia: an electron microscopic study. J Morphol 1965;117(03):467–537

68 De Bruyn PPH, Breen PC, Thomas TB. The microcirculation of the bone marrow. Anat Rec 1970;168(01):55–68

69 Chen WT, Shih TTF, Chen RC, et al. Vertebral bone marrow perfusion evaluated with dynamic contrast-enhanced MR imaging: significance of aging and sex. Radiology 2001;220(01): 213–218

70 Zhang X, Pang H, Dong Y, et al. A study of dynamic contrast-enhanced MR imaging features and influence factors of pelvic bone marrow in adult females. Osteoporos Int 2019;30(12):2469–2476

71 Breault SR, Heye T, Bashir MR, et al. Quantitative dynamic contrast-enhanced MRI of pelvic and lumbar bone marrow: effect of age and marrow fat content on pharmacokinetic parameter values. AJR Am J Roentgenol 2013;200(03):W297-303

72 Guan Y, Peck KK, Lyo J, et al. T1-weighted dynamic contrast-enhanced MRI to differentiate nonneoplastic and malignant vertebral body lesions in the spine. Radiology 2020;297(02): 382–389

73 Arevalo-Perez J, Peck KK, Lyo JK, Holodny AI, Lis E, Karimi S. Differentiating benign from malignant vertebral fractures using T1 -weighted dynamic contrast-enhanced MRI. J Magn Reson Imaging 2015;42(04):1039–1047

74 Liao D, Xie L, Han Y, et al. Dynamic contrast-enhanced magnetic resonance imaging for differentiating osteomyelitis from acute neuropathic arthropathy in the complicated diabetic foot. Skeletal Radiol 2018;47(10):1337–1347

75 Zampa V, Bargellini I, Rizzo L, et al. Role of dynamic MRI in the follow-up of acute Charcot foot in patients with diabetes mellitus. Skeletal Radiol 2011;40(08):991–999

76 Fei ZP, Fei QP, Niu H, Wu J, Ming NG. Application of dynamic contrast enhanced MRI in the diagnosis of brucellar spondylitis. Radiol Infect Dis 2019;6(02):54–60

77 Qiao P, Zhao P, Gao Y, Bai Y, Niu G. Differential study of DCE-MRI parameters in spinal metastatic tumors, brucellar spondylitis and spinal tuberculosis. Chin J Cancer Res 2018;30(04):425–431

78 Verma M, Sood S, Singh B, Thakur M, Sharma S. Dynamic contrast-enhanced magnetic resonance perfusion volumetrics can differentiate tuberculosis of the spine and vertebral malignancy. Acta Radiol 2021;63(11):1504–1512

79 Lang N, Su MY, Yu HJ, Yuan H. Differentiation of tuberculosis and metastatic cancer in the spine using dynamic contrast-enhanced MRI. Eur Spine J 2015;24(08):1729–1737

80 Albano D, Bruno F, Agostini A, et al; Young SIRM Working Group. Dynamic contrast-enhanced (DCE) imaging: state of the art and applications in whole-body imaging. Jpn J Radiol 2022;40(04): 341–366

81 Chiabai O, Van Nieuwenhove S, Vekemans MC, et al. Whole-body MRI in oncology: can a single anatomic T2 Dixon sequence replace the combination of T1 and STIR sequences to detect skeletal metastasis and myeloma? Eur Radiol 2023;33(01):244–257

82 Delgado J, Chauvin NA, Bedoya MA, Patel SJ, Anupindi SA. Whole-body magnetic resonance imaging in the evaluation of children with fever without a focus. Pediatr Radiol 2021;51(04):605–613

83 Tavakoli AA, Reichert M, Blank T, et al. Findings in whole body MRI and conventional imaging in patients with fever of unknown origin—a retrospective study. BMC Med Imaging 2020;20(01):94

84 Voit AM, Arnoldi AP, Douis H, et al. Whole-body magnetic resonance imaging in chronic recurrent multifocal osteomyelitis: clinical longterm assessment may underestimate activity. J Rheumatol 2015;42(08):1455–1462

85 Andronikou S, Kraft JK, Offiah AC, et al. Whole-body MRI in the diagnosis of paediatric CNO/CRMO. Rheumatology (Oxford) 2020;59(10):2671–2680

86 Kieninger A, Schäfer JF, Tsiflikas I, et al. Early diagnosis and response assessment in chronic recurrent multifocal osteomyelitis: changes in lesion volume and signal intensity assessed by whole-body MRI. Br J Radiol 2022;95(1130):20211091

87 Arnoldi AP, Schlett CL, Douis H, et al. Whole-body MRI in patients with non-bacterial osteitis: radiological findings and correlation with clinical data. Eur Radiol 2017;27(06):2391–2399

88 Roderick M, Shah R, Finn A, Ramanan AV. Efficacy of pamidronate therapy in children with chronic non-bacterial osteitis: disease activity assessment by whole body magnetic resonance imaging. Rheumatology (Oxford) 2014;53(11):1973–1976

89 Bhat CS, Roderick M, Sen ES, Finn A, Ramanan AV. Efficacy of pamidronate in children with chronic non-bacterial osteitis using whole body MRI as a marker of disease activity. Pediatr Rheumatol Online J 2019;17(01):35

90 Wang L, Sun B, Li C. Clinical and radiological remission of osteoarticular and cutaneous lesions in SAPHO patients treated with secukinumab: a case series. J Rheumatol 2021;48(06): 953–955

91 Lecouvet FE, Vander Maren N, Collette L, et al. Whole body MRI in spondyloarthritis (SpA): preliminary results suggest that DWI outperforms STIR for lesion detection. Eur Radiol 2018;28(10): 4163–4173

92 Althoff CE, Sieper J, Song I-H, et al. Comparison of clinical examination versus whole-body magnetic resonance imaging of enthesitis in patients with early axial spondyloarthritis during 3 years of continuous etanercept treatment. J Rheumatol 2016; 43(03):618–624

93 Giraudo C, Lecouvet FE, Cotten A, et al. Whole-body magnetic resonance imaging in inflammatory diseases: where are we now? Results of an international survey by the European Society of Musculoskeletal Radiology. Eur J Radiol 2021;136:109533

94 Østergaard M, Eshed I, Althoff CE, et al. Whole-body magnetic resonance imaging in inflammatory arthritis: systematic literature review and first steps toward standardization and an OMERACT scoring system. J Rheumatol 2017;44(11):1699–1705

95 Krabbe S, Østergaard M, Eshed I, et al. Whole-body magnetic resonance imaging in axial spondyloarthritis: reduction of sacroiliac, spinal, and entheseal inflammation in a placebo-controlled trial of adalimumab. J Rheumatol 2018;45(05):621–629

96 Weckbach S, Schewe S, Michaely HJ, Steffinger D, Reiser MF, Glaser C. Whole-body MR imaging in psoriatic arthritis: additional value for therapeutic decision making. Eur J Radiol 2011; 77(01):149–155

97 Song IH, Hermann K, Haibel H, et al. Effects of etanercept versus sulfasalazine in early axial spondyloarthritis on active inflammatory lesions as detected by whole-body MRI (ESTHER): a 48-week randomised controlled trial. Ann Rheum Dis 2011;70(04): 590–596

98 Krabbe S, Eshed I, Sørensen IJ, et al. Novel whole-body magnetic resonance imaging response and remission criteria document diminished inflammation during golimumab treatment in axial spondyloarthritis. Rheumatology (Oxford) 2020;59(11): 3358–3368

99 Poll LW, Cox ML, Godehardt E, Steinhof V, vom Dahl S. Whole body MRI in type I Gaucher patients: evaluation of skeletal involvement. Blood Cells Mol Dis 2011;46(01):53–59

100 Yokota S, Sakamoto K, Shimizu Y, et al. Evaluation of whole-body modalities for diagnosis of multifocal osteonecrosis—a pilot study. Arthritis Res Ther 2021;23(01):83

101 Herrmann J, Afat S, Brendlin A, Chaika M, Lingg A, Othman AE. Clinical evaluation of an abbreviated contrast-enhanced whole-body MRI for oncologic follow-up imaging. Diagnostics (Basel) 2021;11(12):2368

102 Lecouvet FE, Pasoglou V, Van Nieuwenhove S, et al. Shortening the acquisition time of whole-body MRI: 3D T1 gradient echo Dixon vs fast spin echo for metastatic screening in prostate cancer. Eur Radiol 2020;30(06):3083–3093

103 Machann J, Stefan N, Schick F. (1)H MR spectroscopy of skeletal muscle, liver and bone marrow. Eur J Radiol 2008;67(02):275–284

104 Ecklund K, Vajapeyam S, Mulkern RV, et al. Bone marrow fat content in 70 adolescent girls with anorexia nervosa: magnetic resonance imaging and magnetic resonance spectroscopy assessment. Pediatr Radiol 2017;47(08):952–962

105 Badr S, Legroux-Gérot I, Vignau J, et al. Comparison of regional bone marrow adiposity characteristics at the hip of underweight and weight-recovered women with anorexia nervosa using magnetic resonance spectroscopy. Bone 2019;127:135–145

106 Degnan AJ, Ho-Fung VM, Wang DJ, Ficicioglu C, Jaramillo D. Gaucher disease status and treatment assessment: pilot study using magnetic resonance spectroscopy bone marrow fat fractions in pediatric patients. Clin Imaging 2020;63:1–6

107 Yuan W, Lei Y, Tang C, et al. Quantification of bone marrow edema in rheumatoid arthritis by using high-speed T2-corrected multiecho acquisition of ^{1}H magnetic resonance spectroscopy: a feasibility study. Clin Rheumatol 2021;40(11):4639–4647

108 Oriol A, Valverde D, Capellades J, Cabañas ME, Ribera JM, Arús C. In vivo quantification of response to treatment in patients with multiple myeloma by 1H magnetic resonance spectroscopy of bone marrow. MAGMA 2007;20(02):93–101

109 Bolacchi F, Uccioli L, Masala S, et al. Proton magnetic resonance spectroscopy in the evaluation of patients with acute Charcot neuro-osteoarthropathy. Eur Radiol 2013;23(10):2807–2813

110 Lee SH, Yoo HJ, Yu SM, Hong SH, Choi JY, Chae HD. Fat quantification in the vertebral body: comparison of modified Dixon technique with single-voxel magnetic resonance spectroscopy. Korean J Radiol 2019;20(01):126–133

111 Park S, Kwack KS, Chung NS, Hwang J, Lee HY, Kim JH. Intravoxel incoherent motion diffusion-weighted magnetic resonance imaging of focal vertebral bone marrow lesions: initial experience of the differentiation of nodular hyperplastic hematopoietic bone marrow from malignant lesions. Skeletal Radiol 2017;46 (05):675–683

112 Jo A, Jung JY, Lee SY, et al. Prognosis prediction in initially diagnosed multiple myeloma patients using intravoxel incoherent motion-diffusion weighted imaging and multiecho Dixon imaging. J Magn Reson Imaging 2021;53(02):491–501

113 Omoumi P, Becce F, Racine D, Ott JG, Andreisek G, Verdun FR. Dual-energy CT: basic principles, technical approaches, and applications in musculoskeletal imaging (Part 1). Semin Musculoskelet Radiol 2015;19(05):431–437

114 Omoumi P, Zufferey P, Malghem J, So A. Imaging in gout and other crystal-related arthropathies. Rheum Dis Clin North Am 2016;42 (04):621–644

115 Omoumi P, Verdun FR, Guggenberger R, Andreisek G, Becce F, Dual-Energy CT. Dual-energy CT: basic principles, technical approaches, and applications in musculoskeletal imaging (Part 2). Semin Musculoskelet Radiol 2015;19(05):438–445

116 Willemink MJ, Persson M, Pourmorteza A, Pelc NJ, Fleischmann D. Photon-counting CT: technical principles and clinical prospects. Radiology 2018;289(02):293–312

117 Esquivel A, Ferrero A, Mileto A, et al. Photon-counting detector CT: key points radiologists should know. Korean J Radiol 2022;23 (09):854–865

118 Rajendran K, Petersilka M, Henning A, et al. First clinical photon-counting detector CT system. 2022;303(01):130–138

119 Arentsen L, Yagi M, Takahashi Y, et al. Validation of marrow fat assessment using noninvasive imaging with histologic examination of human bone samples. Bone 2015;72:118–122

120 Cheraya G, Sharma S, Chhabra A. Dual energy CT in musculoskeletal applications beyond crystal imaging: bone marrow maps and metal artifact reduction. Skeletal Radiol 2022;51(08):1521–1534

121 Kosmala A, Weng AM, Heidemeier A, et al. Multiple myeloma and dual-energy CT: diagnostic accuracy of virtual noncalcium technique for detection of bone marrow infiltration of the spine and pelvis. Radiology 2018;286(01):205–213

122 Abdullayev N, Große Hokamp N, Lennartz S, et al. Improvements of diagnostic accuracy and visualization of vertebral metastasis using multi-level virtual non-calcium reconstructions from dual-layer spectral detector computed tomography. Eur Radiol 2019;29(11):5941–5949

123 Yuan Y, Zhang Y, Lang N, Li J, Yuan H. Differentiating malignant vertebral tumours from non-malignancies with CT spectral imaging: a preliminary study. Eur Radiol 2015;25(10):2945–2950
124 Dong Y, Zheng S, Machida H, et al. Differential diagnosis of osteoblastic metastases from bone islands in patients with lung cancer by single-source dual-energy CT: advantages of spectral CT imaging. Eur J Radiol 2015;84(05):901–907
125 Zheng S, Dong Y, Miao Y, et al. Differentiation of osteolytic metastases and Schmorl's nodes in cancer patients using dual-energy CT: advantage of spectral CT imaging. Eur J Radiol 2014; 83(07):1216–1221
126 Yuan Y, Lang N, Yuan H. Rapid-kilovoltage-switching dual-energy computed tomography (CT) for differentiating spinal osteolytic metastases from spinal infections. Quant Imaging Med Surg 2021;11(02):620–627
127 Cavallaro M, D'Angelo T, Albrecht MH, et al. Comprehensive comparison of dual-energy computed tomography and magnetic resonance imaging for the assessment of bone marrow edema and fracture lines in acute vertebral fractures. Eur Radiol 2022; 32(01):561–571
128 Wang CK, Tsai JM, Chuang MT, Wang MT, Huang KY, Lin RM. Bone marrow edema in vertebral compression fractures: detection with dual-energy CT. Radiology 2013;269(02):525–533
129 Akisato K, Nishihara R, Okazaki H, et al. Dual-energy CT of material decomposition analysis for detection with bone marrow edema in patients with vertebral compression fractures. Acad Radiol 2020;27(02):227–232
130 Pan J, Yan L, Gao H, et al. Fast kilovoltage (KV)-switching dual-energy computed tomography hydroxyapatite (HAP)-water decomposition technique for identifying bone marrow edema in vertebral compression fractures. Quant Imaging Med Surg 2020; 10(03):604–611
131 Frellesen C, Azadegan M, Martin SS, et al. Dual-energy computed tomography-based display of bone marrow edema in incidental vertebral compression fractures: diagnostic accuracy and characterization in oncological patients undergoing routine staging computed tomography. Invest Radiol 2018;53(07):409–416
132 Ghazi Sherbaf F, Sair HI, Shakoor D, et al. DECT in detection of vertebral fracture-associated bone marrow edema: a systematic review and meta-analysis with emphasis on technical and imaging interpretation parameters. Radiology 2021;300(01):110–119
133 Foti G, Serra G, Iacono V, Zorzi C. Identification of traumatic bone marrow oedema: the pearls and pitfalls of dual-energy CT (DECT). Tomography 2021;7(03):424–433
134 Wilson MP, Lui K, Nobbee D, et al. Diagnostic accuracy of dual-energy CT for the detection of bone marrow edema in the appendicular skeleton: a systematic review and meta-analysis. Eur Radiol 2021;31(03):1558–1568
135 Narayanan A, Dettori N, Chalian M, Xi Y, Komarraju A, Chhabra A. Dual-energy CT-generated bone marrow oedema maps improve timely visualisation and recognition of acute lower extremity fractures. Clin Radiol 2021;76(09):710.e9–710.e14
136 Kellock TT, Nicolaou S, Kim SSY, et al. Detection of bone marrow edema in nondisplaced hip fractures: utility of a virtual non-calcium dual-energy CT application. Radiology 2017;284(03): 798–805
137 Reddy T, McLaughlin PD, Mallinson PI, et al. Detection of occult, undisplaced hip fractures with a dual-energy CT algorithm targeted to detection of bone marrow edema. Emerg Radiol 2015;22(01):25–29
138 Jang SW, Chung BM, Kim WT, Gil JR. Nondisplaced fractures on hip CT: added value of dual-energy CT virtual non-calcium imaging for detection of bone marrow edema using visual and quantitative analyses. Acta Radiol 2019;60(11):1465–1473
139 Palm HG, Lang P, Hackenbroch C, Sailer L, Friemert B. Dual-energy CT as an innovative method for diagnosing fragility fractures of the pelvic ring: a retrospective comparison with MRI as the gold standard. Arch Orthop Trauma Surg 2020;140 (04):473–480
140 Gosangi B, Mandell JC, Weaver MJ, et al. Bone marrow edema at dual-energy CT: a game changer in the emergency department. Radiographics 2020;40(03):859–874
141 Issa G, Mulligan M. Dual energy CT can aid in the emergent differentiation of acute traumatic and pathologic fractures of the pelvis and long bones. Emerg Radiol 2020;27(03):285–292
142 Wu H, Zhang G, Shi L, et al. Axial spondyloarthritis: dual-energy virtual noncalcium CT in the detection of bone marrow edema in the sacroiliac joints. Radiology 2019;290(01):157–164
143 Chen M, Herregods N, Jaremko JL, et al. Bone marrow edema in sacroiliitis: detection with dual-energy CT. Eur Radiol 2020;30 (06):3393–3400
144 Chen Z, Chen Y, Zhang H, Jia X, Zheng X, Zuo T. Diagnostic accuracy of dual-energy computed tomography (DECT) to detect non-traumatic bone marrow edema: a systematic review and meta-analysis. Eur J Radiol 2022;153:110359
145 Bierry G, Venkatasamy A, Kremer S, Dosch JC, Dietemann JL. Dual-energy CT in vertebral compression fractures: performance of visual and quantitative analysis for bone marrow edema demonstration with comparison to MRI. Skeletal Radiol 2014; 43(04):485–492
146 Petritsch B, Kosmala A, Weng AM, et al. Vertebral compression fractures: third-generation dual-energy CT for detection of bone marrow edema at visual and quantitative analyses. Radiology 2017;284(01):161–168
147 Marin D, Boll DT, Mileto A, Nelson RC. State of the art: dual-energy CT of the abdomen. Radiology 2014;271(02):327–342
148 Foti G, Beltramello A, Catania M, Rigotti S, Serra G, Carbognin G. Diagnostic accuracy of dual-energy CT and virtual non-calcium techniques to evaluate bone marrow edema in vertebral compression fractures. Radiol Med (Torino) 2019;124(06):487–494
149 Lauri C, Tamminga M, Glaudemans AWJM, et al. Detection of osteomyelitis in the diabetic foot by imaging techniques: a systematic review and meta-analysis comparing MRI, white blood cell scintigraphy, and FDG-PET. Diabetes Care 2017;40 (08):1111–1120
150 Govaert GAM, Bosch P, IJpma FFA, et al. High diagnostic accuracy of white blood cell scintigraphy for fracture related infections: results of a large retrospective single-center study. Injury 2018; 49(06):1085–1090
151 Gemmel F, Van den Wyngaert H, Love C, Welling MM, Gemmel P, Palestro CJ. Prosthetic joint infections: radionuclide state-of-the-art imaging. Eur J Nucl Med Mol Imaging 2012;39(05): 892–909
152 Lalonde MN, Omoumi P, Prior JO, Zufferey P. Imágenes isotópicas del aparato locomoto [in Spanish]. EMC Aparato Locomotor 2021;54:1–23. Doi: 10.1016/S0246-0521(21)59763-0
153 Glaudemans AWJM, Jutte PC, Cataldo MA, et al. Consensus document for the diagnosis of peripheral bone infection in adults: a joint paper by the EANM, EBJIS, and ESR (with ESCMID endorsement). Eur J Nucl Med Mol Imaging 2019;46(04):957–970
154 Takeuchi M, Dahabreh IJ, Nihashi T, Iwata M, Varghese GM, Terasawa T. Nuclear imaging for classic fever of unknown origin: meta-analysis. J Nucl Med 2016;57(12):1913–1919
155 van Rijsewijk ND, IJpma FFA, Wouthuyzen-Bakker M, Glaudemans AWJM. Molecular imaging of fever of unknown origin: an update. Semin Nucl Med 2023;53(01):4–17
156 Meyer M, Testart N, Jreige M, et al. Diagnostic performance of PET or PET/CT using ^{18}F-FDG labeled white blood cells in infectious diseases: a systematic review and a bivariate meta-analysis. Diagnostics (Basel) 2019;9(02):60
157 Okazaki T, Nakagawa H, Yagi K, Hayase H, Nagahiro S, Saito K. Bone scintigraphy for the diagnosis of the responsible level of osteoporotic vertebral compression fractures in percutaneous balloon kyphoplasty. Clin Neurol Neurosurg 2017;152:23–27

158 Matcuk GR Jr, Mahanty SR, Skalski MR, Patel DB, White EA, Gottsegen CJ. Stress fractures: pathophysiology, clinical presentation, imaging features, and treatment options. Emerg Radiol 2016;23(04):365–375

159 Fan C, Hernandez-Pampaloni M, Houseni M, et al. Age-related changes in the metabolic activity and distribution of the red marrow as demonstrated by 2-deoxy-2-[F-18]fluoro-D-glucose-positron emission tomography. Mol Imaging Biol 2007;9(05): 300–307

160 Agool A, Glaudemans AWJM, Boersma HH, Dierckx RAJO, Vellenga E, Slart RHJA. Radionuclide imaging of bone marrow disorders. Eur J Nucl Med Mol Imaging 2011;38(01):166–178

161 Murata Y, Kubota K, Yukihiro M, Ito K, Watanabe H, Shibuya H. Correlations between 18F-FDG uptake by bone marrow and hematological parameters: measurements by PET/CT. Nucl Med Biol 2006;33(08):999–1004

162 Malla S, Razik A, Das CJ, Naranje P, Kandasamy D, Kumar R. Marrow outside marrow: imaging of extramedullary haematopoiesis. Clin Radiol 2020;75(08):565–578

163 Gosewisch A, Ilhan H, Tattenberg S, et al. 3D Monte Carlo bone marrow dosimetry for Lu-177-PSMA therapy with guidance of non-invasive 3D localization of active bone marrow via Tc-99m-anti-granulocyte antibody SPECT/CT. EJNMMI Res 2019;9(01): 76